

Analytical and numerical study of the nonlinear interaction between a point vortex and a wall-bounded shear layer

By OLIVER V. ATASSI†

Department of Mechanical Engineering, Northwestern University, Evanston, IL 60208, USA

(Received 22 July 1997 and in revised form 19 May 1998)

The unsteady interaction between a vortex and a wall-bounded vorticity layer is studied as a model for transport and mixing between rotational and irrotational flows. The problem is formulated in terms of contour integrals and a kinematic condition along the interface which demarcates the vortical and potential regions. Asymptotic solutions are derived for linear, weakly nonlinear and nonlinear long-wave approximations. The solutions show that the initial process of ejection of vorticity into the irrotational flow occurs at a stationary point along the interface. A nonlinear model is derived and shows that such a stationary point is more likely to exist when the circulation of the vortex is counter to the vorticity in the layer. A Lagrangian numerical method based on contour dynamics is then developed for the general nonlinear problem. Two sets of results are presented where for every initial height of the vortex its magnitude and sign are varied. In both sets, it is observed that when the magnitude of the vortex is held constant a much stronger interaction occurs when the sign of the vortex circulation is opposite to that of the vorticity in the layer. Moreover, when the horizontal velocity of the vortex is close to the velocity of the interfacial waves a strong nonlinear interaction between the vortex and the layer ensues and results in the ejection of thin filaments of vorticity into the irrotational flow. In order to study the dynamical consequences of strong unsteady interaction, the wall pressure distribution is computed. The results indicate that a significant rise in the magnitude of the wall pressure is associated with ejection of vorticity from the wall. The present analysis confirms that coherent vortical structures in the outer layer of a turbulent boundary layer can cause ejection of concentrated wall-layer vorticity and explains how and when this process occurs.

1. Introduction

Many basic flows such as boundary layers, mixing layers and jets contain concentrated regions of vorticity which interact with each other and the surrounding irrotational flow (Roshko 1976; Falco 1977). The deterministic evolution and interaction of these coherent structures have a significant effect on momentum and heat transport properties. In turbulent boundary layers, for example, the unsteady interactions between these regions are important in the exchange of momentum between the outer layer and wall regions. The causative element (Robinson 1991) in the momentum transport and mixing properties of the boundary layer is the interaction between the outer vortices and the shear layers. Ejection and entrainment are the nonlinear phenomena which are the manifestations of this transport.

† Pratt & Whitney, Aero/CFD Group, E. Hartford, CT 06108, USA.

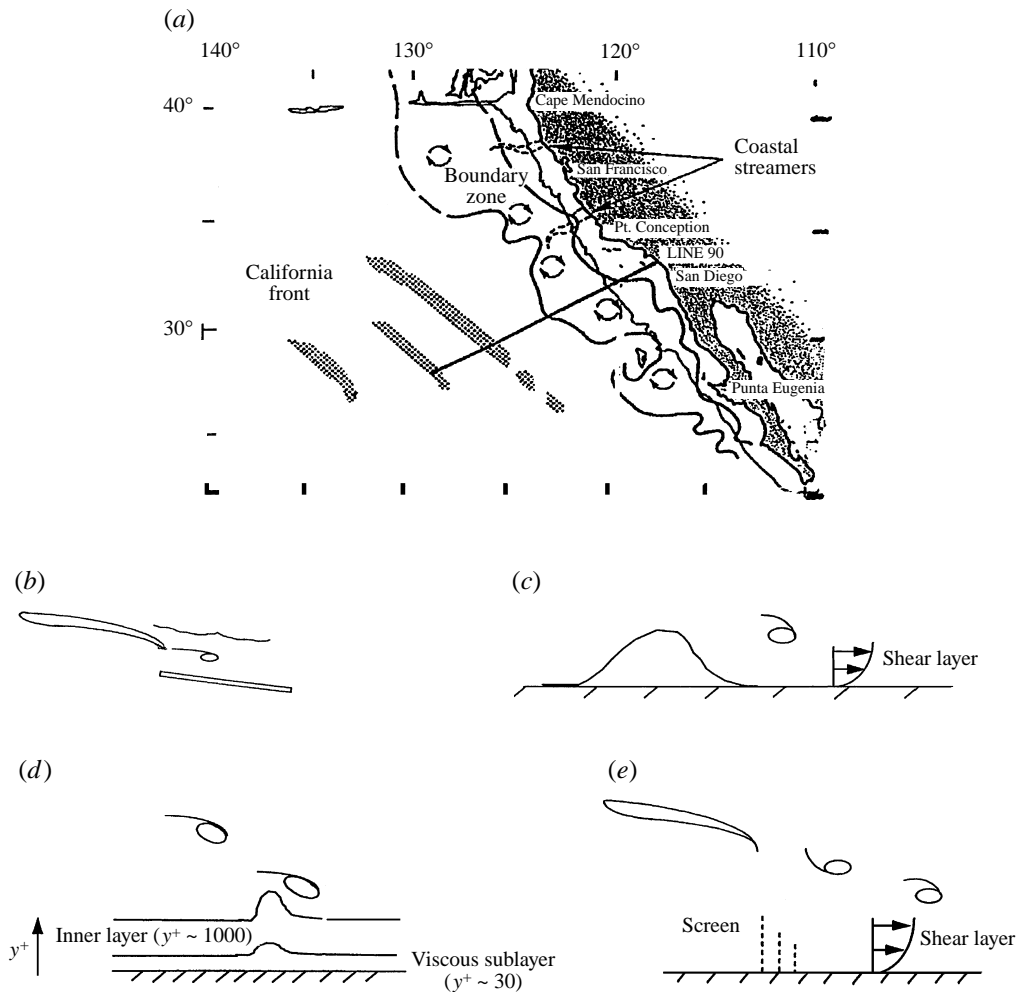


FIGURE 1. Five examples showing the interaction of a vortex with a wall-bounded shear layer. (a) Eddies off the California coast interacting with coastal currents transport fluid away from the coast and out to the ocean (taken from Liu *et al.* 1988). (b) A vortex shed from the trailing edge of a wing (during takeoff or landing) passing over a flap. (c) A vortex shed from a bluff body interacts with the Earth boundary layer as it convects downstream. (d) A sketch of a turbulent boundary layer where an eddy in the outer layer initiates ejection of vorticity from the wall region (Falco 1991). (e) A schematic of an experiment for the interaction of a patch of vorticity with a wall-bounded shear flow. A screen creates a shear flow along a plate. The characteristics and thickness of the shear flow are determined by the screen design. Above a vortex is shed from an airfoil and convects downstream interacting with the wall-bounded shear layer.

In figure 1, we present examples of physical flows occurring in nature or experiment where concentrated patches of vorticity interact with a wall-bounded shear layer. Figure 1(a) is a schematic taken from Liu, Simpson and Schedvin (1988) showing a system of eddies off the California coast interacting with coastal currents. Note the presence of coastal streamers indicating strong momentum transport via this inviscid interaction. These geophysical observations (see also Ikeda & Apel 1981) have motivated several studies of the vortex/shear layer interaction (Stern & Pratt 1985; Stern & Flierl 1987; Bell 1990). Figure 1(b) shows vortices shed from the trailing

edge of a wing and interacting with flaps extended during takeoff and landing. The spanwise vortices are shed in response to unsteady effects such as manoeuvring or upstream turbulence and are convected downstream in the wake of the wing (sheared flow) passing close to the flap surface. Figure 1(c) shows another example where vorticity is shed from the edge of a bluff body such as a mountain ridge or a wide building. This vorticity then interacts with the Earth boundary layer as it propagates downstream. A schematic of a turbulent boundary (figure 1d) layer as suggested by Falco's experiments (1991) presents another example of vorticity interacting with wall-bounded shear layers. Each of these examples occurs in high Reynolds number flow where most of the flow is inviscid but rotational and where viscous effects are confined to a thin sublayer near the wall. The objective of the present paper is to examine the nonlinear but inviscid interaction between a concentrated patch of vorticity and a wall-bounded shear layer. A model for this generic problem can be reproduced in a laboratory experiment as shown in figure 1(e). A screen placed upstream creates a sheared flow along a plate. The characteristics and thickness of the sheared flow are determined by the screen design. A vortex is then shed from the trailing edge of an airfoil in response to an abrupt unsteady motion.

The interaction of vorticity with a wall-bounded shear layer has been extensively investigated in the context of turbulent boundary layers. These experiments have motivated the parameter range studied in this paper and a brief summary of the important experimental results is given. It has been hypothesized that strong interaction between the vortical (inner) flow in the wall region and concentrated regions of vorticity in the mainly irrotational (outer) region result in mixing of fluid between the two regions (Falco 1991). Falco concluded that the coherent motions can be divided into two groups. One whose dynamics are largely independent of the wall and lie in the outer region. The second group lies in the wall region and is dependent upon the high shear and impermeability of the wall. The outer region motions initiate ejection of wall region fluid into the outer layer. In addition, Falco observed, using statistical two-point vorticity correlations, that an important feature of this interaction is that the portion of the outer region structure closest to the wall had spanwise vorticity whose sense of rotation was opposite to the mean spanwise vorticity in the wall region layer. Myose & Blackwelder (1994) studied the interaction between experimentally generated spanwise vortical eddies and low-speed streaks in the wall region. They also found that the sign of the spanwise outer region eddies was an important factor in determining whether the interaction resulted in ejection of wall region fluid into the outer layer. Note that the viscous sublayer extends to about $y^+ \approx 30$ and the inner layer extends to $y^+ \approx 1000$ – $10\,000$, where $y^+ = y(\tau_w/\rho)^{1/2}/\nu$ is the coordinate normal to the wall non-dimensionalized by the kinematic viscosity and the wall shear. This suggests that the inviscid interaction mechanism, which is the subject of the present paper, is important in the inner layer–outer layer interaction.

The simple model we consider here is a wall-bounded uniform shear layer interacting with a point vortex. In the present work we determine how a vortex placed in the irrotational flow may enhance or subdue the momentum transfer between a wall-bounded shear layer and an irrotational flow. Toward this end, we (i) describe the physical processes involved in the nonlinear, unsteady interaction between the layer of vorticity and the vortex and (ii) determine the conditions under which substantial and rapid ejection of vorticity from the shear layer occurs. In particular, we examine both analytically and numerically two sets of results motivated by two physical problems: the vortex/shear layer interaction when a vortex shed from an airfoil or bluff body passes over a wall-bounded shear layer (figure 1b, c, e) and the interaction of outer

layer vortices in a turbulent boundary layer with the wall-layer vorticity (figure 1*d*). The order of magnitude estimates for the vortex strength and height suggested by these physical problems are presented in §4.1.

The evolution of regions of constant vorticity (uniform shear) in two-dimensional, incompressible, inviscid flows have been extensively investigated using contour dynamics. The assumption of uniform vorticity allows one to solve Euler's equations in terms of integrals along an interface separating different regions of constant vorticity (see Zabusky, Hughes & Roberts 1979). The numerical solution calculates the Lagrangian evolution of the interface which corresponds to a line of discontinuous vorticity. As a result of the discontinuous distribution of vorticity and the neglect of viscosity, scales develop which are too small to resolve at some finite time. Dritschel (1988) has devised a scheme for extending contour dynamics calculations by limiting the formation of scales which lie below a prescribed cutoff limit. This allowed him to extend his computations for long times in order to investigate the long-time state of vortex interactions between patches of uniform vorticity (Dritschel & Legras 1993).

Contour dynamics models have been utilized to study a wide variety of flows ranging from geophysical flows to boundary layers and jets. Pullin (1981) first computed the evolution of a wall-bounded layer of uniform vorticity subject to periodic, finite-amplitude disturbances. His numerical results showed the development of overturning disturbances which entrained irrotational flow into the layer. Stern & Pratt (1985) showed that finite-amplitude disturbances to a thin, wall-bounded layer of vorticity steepened and the formation of propagating vorticity fronts occurred. Jimenez & Orlandi (1993) considered the same model and further focused on the thin layer limit. Their results indicated that under certain conditions the layer rolls up and breaks into compact vortices which propagate downstream at constant speed. In order to study unsteady effects that occur when a localized region of vorticity interacts with a layer of vorticity Bell (1990) and Atassi, Bernoff & Lichter (1997) studied the interaction between a point vortex and a layer of constant vorticity. This work focused on cases where the vortex was weak compared to the vorticity in the layer and thus the disturbances to the layer were small. Under these conditions, the unsteady interaction modified the linear behaviour of the system when the vortex propagated with a speed equal to that of the interfacial waves. In this case, a strong interaction between the vortex and the layer of vorticity resulted and growing and steepening disturbances ensued.

In the present investigation, we are interested in the mechanisms involved in the vortex-induced ejection of vorticity from the wall and the effect of varying the sign of the vortex circulation. Consequently, we consider cases where the inertia (circulation) of the vortex is large (but either positive or negative) compared to that of the vorticity layer. We do not consider three-dimensional effects which are an important feature of turbulent flows. Instead, we focus on understanding in detail the interaction between a vortex and a layer of vorticity with the aim of showing the importance and properties of this interaction in the transfer of momentum between a vortical region lying near a wall and a mainly irrotational flow lying above it.

In §2, we present the general formulation of the model. The full nonlinear problem is formulated in terms of the Lagrangian evolution of the interface separating vortical and irrotational flow. Section 3 develops a thin layer theory and studies the various limiting cases which arise depending upon the strength of the vortex relative to that of the layer. We show that a variety of solutions to this interaction exist ranging from propagating solitary waves to strong unsteady interactions which result in the ejection and rollup of vorticity into the irrotational flow. Moreover, we show that

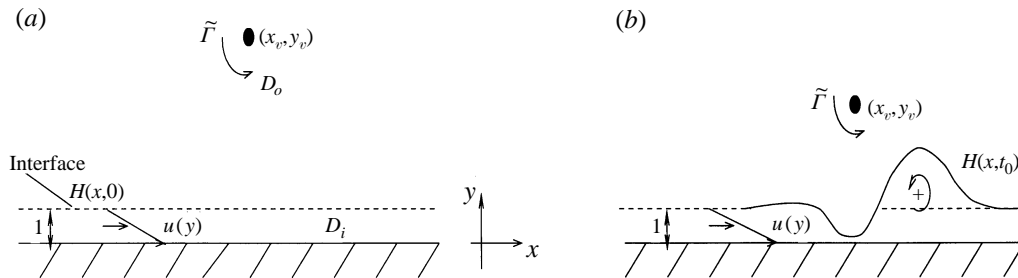


FIGURE 2. Schematic of the model problem studying the interaction between a point vortex with a wall-bounded layer of piecewise-uniform vorticity. (a) The assumed initial state of the system. An unperturbed uniform, wall-bounded shear layer is forced by a vortex which lies above it. (b) After some time, t_0 , the interface deforms due to the velocity induced by the vortex. Subsequently, the vortex is displaced by the deformation of the interface.

strong interaction is much more likely to occur when the circulation of the vortex is counter to that of the vorticity layer. The numerical formulation is shown in §4 and the numerical results for the deformation of the interface and the pathline of the point vortex are presented. These results are compared with the results of §3 and are extended far beyond the validity of the analytical results. Section 5 computes the wall pressure to study the dynamics which result from the kinematics of the interface. Finally §6 discusses and summarizes the conclusions of the work.

2. Formulation

The two-dimensional, incompressible, inviscid flow is decomposed into an inner wall-bounded shear flow D_i with constant vorticity, ω , and an outer region D_o of irrotational flow extending to infinity. A coordinate system (x, y) with the x -axis parallel to the wall and the y -axis perpendicular to it is considered. In this coordinate system, the wall is located at $y = 0$. We choose a frame of reference moving with the velocity U . In this frame of reference, the wall moves downstream with speed U and the fluid velocity goes to zero as $y \rightarrow \infty$. The two regions are separated by the interface located at $y = H(x, t)$. The shear layer extends upstream to $-\infty$ and downstream to $+\infty$ where it has constant thickness H_∞ and thus $\omega = U/H_\infty$. The geometry of the model is shown in figure 2. We non-dimensionalize all lengths with respect to H_∞ , and time with respect to H_∞/U . This yields a non-dimensional vorticity of one.

We briefly describe the formulation of the model. For more details see Pullin (1981) and Atassi *et al.* (1997). The velocity field is the superposition of the velocities induced by the vorticity in the layer and the point vortex in the presence of an impermeable wall. Using a complex representation of the Biot-Savart law, the complex conjugate of the velocity induced by the layer at the observation point $z = x + iy$ is

$$(u(z) - iv(z))_L = \frac{1}{2\pi i} \iint_{D_i} \left[\frac{1}{z - z'} - \frac{1}{z - \bar{z}'} \right] dA' \quad (2.1)$$

where $z' = x' + iy'$ represents the source point and the subscript L denotes the velocity induced by the layer of vorticity. We apply the Area theorem (Milne-Thomson 1968, p. 133) to transform the double integral over the area, D_i , to a line integral over the

contour C enclosing the region D_i . This yields

$$(u - iv)_L = \frac{1}{2\pi i} \left[\oint_C \frac{y' - y}{z' - z} dz' - \oint_C \frac{y' - y}{\bar{z}' - z} d\bar{z}' \right], \quad (2.2)$$

where the direction of integration is chosen to be counterclockwise. The assumption of finite thickness, H_∞ as $|x| \rightarrow \infty$, ensures that the velocity field is finite. These integrals can be evaluated analytically for a shear layer of constant thickness. Thus the numerical quadrature is limited to the perturbed part of the contour. The expression for the velocity, equation (2.2), is suitable for accurate numerical quadrature because it no longer involves a singular kernel.

Adding to (2.2) the velocity field induced by the point vortex and its image we obtain

$$u - iv = \frac{1}{2\pi i} \left[\oint_C \frac{y' - y}{z' - z} dz' - \oint_C \frac{y' - y}{\bar{z}' - z} d\bar{z}' \right] + \frac{\tilde{\Gamma}}{2\pi i} \left(\frac{1}{z - z_v} - \frac{1}{z - \bar{z}_v} \right), \quad (2.3)$$

where $z_v(t) = x_v(t) + iy_v(t)$ is the location of the point vortex and the non-dimensional parameter, $\tilde{\Gamma} = \Gamma / (UH_\infty)$, is the ratio of the inertial effects of the vortex with circulation Γ to the inertial effects of the uniform shear layer. Note that due to the image vortex, the vertical velocity at the wall is zero.

The motion of the point vortex depends upon its interaction with the shear layer and its image. Its complex conjugate velocity is given by

$$u(z_v) - iv(z_v) = \frac{d\bar{z}_v}{dt} = \frac{1}{2\pi i} \left[\oint_C \frac{y' - y_v}{z' - z_v} dz' - \oint_C \frac{y' - y_v}{\bar{z}' - z_v} d\bar{z}' \right] + \frac{\tilde{\Gamma}}{4\pi y_v}. \quad (2.4)$$

In addition, conservation of x -momentum may be applied to derive the relation (Bell 1990; Atassi *et al.* 1997)

$$\tilde{\Gamma} [y_v(t) - y_v(0)] = -\frac{1}{2} \int_{-\infty}^{\infty} [H^2(x, t) - H^2(x, 0)] dx. \quad (2.5)$$

Equation (2.5) relates the momentum of the vortex to that of the layer and indicates that the degree of momentum transfer between the inner and outer regions can be related to the vertical displacement of the vortex.

Finally, we specify the initial shape of the interface, $y = H(x, 0) = H_0(x)$ and the kinematic condition that a fluid particle on the interface will remain on the interface,

$$v = \frac{\partial H}{\partial t} + u \frac{\partial H}{\partial x} \quad \text{at} \quad y = H(x, t). \quad (2.6)$$

In summary, the fully nonlinear interaction between the uniform shear layer and the point vortex is formulated in terms of an initial-value problem involving three coupled equations (2.3), (2.4), (2.6). This initial-value problem defining the coupled motions of the interface and the point vortex, in general, must be solved numerically. However, in order to study the different stages of evolution from an initially unperturbed, thin layer to rapidly growing finite-amplitude disturbances, we first examine some limiting cases where the initial thickness of the layer is small compared to the height of the vortex and the interaction between the layer and the vortex is weak. As opposed to stability theory where the primary aim is to determine the conditions where wave-like disturbances grow, this initial-value problem studies how a prescribed initial velocity field evolves in time and determines the conditions which result in the ejection of vorticity into the irrotational flow.

3. Thin layer theory

We consider disturbances to the interface whose variation in the streamwise direction is small relative to the variation in the transverse direction. This implies from (2.4) that the initial height of the point vortex must be large compared to the thickness of the layer, *i.e.* $y_v(0) \gg 1$. In this case, it is possible to derive an analytical expression for the velocity field in terms of the interfacial height, $H(x, t)$, and the velocity induced by the vortex. We then substitute the velocity field induced at the interface into the kinematic condition. This yields the governing equation for the interface. By examining cases where analytical solutions to the kinematic equation may be obtained, we calculate the initial stages of growth of the interface either to the transition to strong inner–outer unsteady interaction leading to ejection of vorticity away from the wall and entrainment of irrotational flow or to the relaxation of the interaction to wave-like behaviour.

3.1. The velocity field induced by the vorticity layer

The velocity field induced by the thin vorticity layer can be derived by considering the stream function, $\psi(x, y, t)$, defined such that

$$u = \frac{\partial \psi}{\partial y} \tag{3.1}$$

and

$$v = -\frac{\partial \psi}{\partial x}. \tag{3.2}$$

Although ψ is continuous across the interface, it is convenient to introduce the notation $\psi^{(I)}$ for the stream function in D_i and $\psi^{(II)}$ for the stream function in D_o . Relating the stream function to the vorticity we obtain

$$\frac{\partial^2 \psi^{(I)}}{\partial x^2} + \frac{\partial^2 \psi^{(I)}}{\partial y^2} = -1, \quad 0 < y < H(x, t), \tag{3.3}$$

and

$$\frac{\partial^2 \psi^{(II)}}{\partial x^2} + \frac{\partial^2 \psi^{(II)}}{\partial y^2} = 0, \quad y > H(x, t). \tag{3.4}$$

To complete this boundary-value problem we must specify conditions at the wall and the interface. By impermeability, the vertical velocity at $y = 0$ must be zero and the velocity goes to zero in the far-field implying

$$\frac{\partial \psi^{(I)}}{\partial x} = 0, \quad y = 0, \tag{3.5}$$

and

$$\frac{\partial \psi^{(II)}}{\partial x} \rightarrow 0 \quad \text{and} \quad \frac{\partial \psi^{(II)}}{\partial y} \rightarrow 0, \quad y \rightarrow \infty. \tag{3.6}$$

At the interface, $y = H(x, t)$, the horizontal and vertical velocities are continuous yielding

$$\frac{\partial \psi^{(I)}}{\partial x} = \frac{\partial \psi^{(II)}}{\partial x} \tag{3.7}$$

and

$$\frac{\partial \psi^{(I)}}{\partial y} = \frac{\partial \psi^{(II)}}{\partial y}. \tag{3.8}$$

Since the flow is irrotational in D_o , we can use Cauchy's formula to express the complex conjugate of the velocity in terms of its expression along the interface \mathcal{L} ,

$$(u - iv)^{(II)} = \frac{1}{2\pi i} \int_{\mathcal{L}} \frac{(u - iv)^{(I)}}{z' - z} dz' \quad (3.9)$$

where $z' \in \mathcal{L}$. In the inner (shear) layer and the region of the outer (irrotational) layer where the distance above the interface is small compared to the long-wavelength disturbances on the interface, the streamwise variation of the flow field is small relative to the variation in the transverse direction. To represent this, we introduce the slow variable $X = \epsilon x$ where $0 < \epsilon \ll 1$. As a result, at the interface, $y = H(X, t)$ and the kinematic condition becomes

$$v = \frac{\partial H}{\partial t} + \epsilon u \frac{\partial H}{\partial X}. \quad (3.10)$$

Near the interface, the variation in x is small compared to that in y ; however far above the layer the variation in x and y may be of the same order. Hence, in order to obtain a solution which is uniformly valid in D_i and D_o , we must solve equations (3.3) and (3.4) with the conditions (3.5)–(3.8).

To this end, we expand the stream function and the velocity field in powers of ϵ ,

$$\psi^{(II)} = \psi_{(0)}^{(II)} + \epsilon \psi_{(1)}^{(II)} + \dots, \quad (3.11)$$

$$(u - iv)^{(II)} = (u - iv)_{(0)}^{(II)} + \epsilon (u - iv)_{(1)}^{(II)} + \dots. \quad (3.12)$$

Using these expansions we determine the velocity field to $O(\epsilon)$ for three different cases of the scaling of y_v and $\tilde{\Gamma}$ in terms of ϵ . Note that this expansion results from the long-wave assumption, $\partial H / \partial x = O(\epsilon)$. Although $H(x, t)$ may appear locally constant for finite variation of $x = O(1)$, $\partial H / \partial X = O(1)$ and $H(X, t)$ is not constant for variations of $X = O(1)$. For example, if $H = 1 + H_1 e^{-X^2}$, H varies from $H_1 + 1$ to 1. For the small-amplitude case treated in § 3.3.1, it is further assumed that $H_1 = O(\epsilon)$.

3.1.1. Case I: $\tilde{\Gamma} = O(1)$ and $y_v \gg O(1/\epsilon)$

When the vortex strength is finite and the vortex very far above the layer, $y_v \gg O(1/\epsilon)$, the velocity induced by the vortex on the layer is $o(\epsilon)$ and the velocity field produced by the deformation of the layer is due solely to its self-interaction.

The leading-order term of the expansion (3.11) in the inner region, $\psi_{(0)}^{(I)}$, must satisfy

$$\frac{\partial^2 \psi_{(0)}^{(I)}}{\partial y^2} = -1 \quad (3.13)$$

and the boundary condition

$$\frac{\partial \psi_{(0)}^{(I)}}{\partial x} = 0 \quad \text{at } y = 0. \quad (3.14)$$

This suggests that

$$\psi_{(0)}^{(I)} = -\frac{y^2}{2} + a_1(X, t)y. \quad (3.15)$$

As a result,

$$u_{(0)}^{(I)} = -y + a_1(X, t) \quad (3.16)$$

and

$$v_{(0)}^{(I)} = 0. \tag{3.17}$$

Note that since $u_{(0)}^{(I)}$ vanishes at the interface for large $|x|$, $a_1(X, t) \rightarrow 1$ as $|x| \rightarrow \infty$.

We now determine the expression for the leading-order term of expansion (3.11), $\psi^{(II)}$, in the outer region D_o . Since for $y > H(X, t)$ the flow is irrotational, $(u - iv)^{(II)}$ is an analytic function of the complex variable z . Applying Cauchy's integral formula, using conditions (3.6)–(3.8) and evaluating the velocity on the interface we obtain

$$(u - iv)_{(0)}^{(II)} = \frac{1}{2}(u - iv)_{(0)}^{(I)} + \frac{1}{2\pi i} \oint_{-\infty}^{\infty} \frac{(u - iv)_{(0)}^{(I)}}{(X' - X)} dX', \tag{3.18}$$

where the integral in (3.18) is a Cauchy principal value.

Since by continuity of the velocity (3.7) and (3.8), $v_{(0)}^{(II)} = v_{(0)}^{(I)} = 0$, equation (3.18) implies that $u_{(0)}^{(II)} = 0$ and $u_{(0)}^{(I)} = 0$. Therefore, equation (3.16) at the interface yields

$$a_1(X, t) = H(X, t). \tag{3.19}$$

The leading-order expansion of the velocity is then

$$u_{(0)}^{(I)} = H(X, t) - y, \quad v_{(0)}^{(I)} = 0, \quad u_{(0)}^{(II)} = 0, \quad v_{(0)}^{(II)} = 0. \tag{3.20}$$

The $O(\epsilon)$ expansion of $\psi(x, y, t)$ in the inner region must satisfy

$$\frac{\partial^2 \psi_{(1)}^{(I)}}{\partial y^2} = 0 \tag{3.21}$$

and

$$\frac{\partial \psi_{(1)}^{(I)}}{\partial x} = 0 \quad \text{at } y = 0. \tag{3.22}$$

Hence,

$$\psi_{(1)}^{(I)} = a_2(X, t)y \tag{3.23}$$

and

$$u_{(1)}^{(I)} = a_2(X, t), \quad v_{(1)}^{(I)} = -y \frac{\partial H}{\partial X}, \tag{3.24}$$

where $a_2(X, t)$ is a function to be determined.

For the outer solution, we again use Cauchy's integral formula and since $(u - iv)_0 = 0$ on the interface the only contribution at $O(\epsilon)$ is

$$(u - iv)_{(1)}^{(II)} = \frac{1}{2\pi i} \int_{\mathcal{L}} \frac{(u - iv)_{(1)}^{(I)}}{(z' - z)} dz', \quad z \in D_o. \tag{3.25}$$

In order to determine $a_2(X, t)$, we consider the $O(\epsilon)$ expansion of the outer velocity lying an $O(1)$ distance above the interface. Using Hilbert's inversion formula to express (3.25) in terms of the vertical velocity at the interface and where y is $O(1)$, we obtain

$$u_{(1)}^{(II)} = \frac{1}{\pi} \oint_{-\infty}^{\infty} \frac{H(X', t)[\partial H(X', t)/\partial X']}{(X' - X)} dX'. \tag{3.26}$$

Using (3.8) and substituting (3.26) into (3.24) gives

$$a_2(X, t) = \frac{1}{\pi} \oint_{-\infty}^{\infty} \frac{H(X', t)[\partial H(X', t)/\partial X']}{(X' - X)} dX'. \tag{3.27}$$

Equation (3.26) corresponds to the Hilbert transform, $\mathcal{H}(-v_{(1)})$, of the vertical velocity and gives the horizontal velocity in D_o in terms of the interfacial height, $H(X, t)$ and its derivative. The velocity field induced far above the interface at a distance $y = O(1/\epsilon)$ has slow variations in both the x - and y -directions. Therefore, we introduce the slow variable $Y = \epsilon y$. The $O(\epsilon)$ velocity far above the interface can then be expressed in terms of the vertical velocity at the interface,

$$(u - iw)_{(1)}^{(II)} = \frac{1}{\pi} \int_{-\infty}^{\infty} \frac{H(X', t)[\partial H(X', t)/\partial X']}{(X' - X) - iY} dX'. \quad (3.28)$$

Note that far above the interface the horizontal and vertical velocity are the same order of magnitude.

The velocity field induced on the vortex by the interface diminishes as their distance apart becomes large and is proportional to the square of the amplitude of the interface. This nonlinear result suggests that disturbances on the interface must propagate at a speed close to that of the vortex or the interaction will wane as the distance between the disturbances and the vortex increases. This idea is consistent with the linear theory (Atassi *et al.* 1997) which showed that a strong vortex–interface interaction only occurred when the phase speed of an interfacial wave coincided with the velocity of the vortex.

3.1.2. Case II: $\tilde{\Gamma} = O(1)$ and $y_v = O(1/\epsilon)$

When the vortex strength is finite and the vortex is somewhat nearer to the layer, $y_v = O(1/\epsilon)$, the effect of the vortex on the layer is $O(\epsilon)$. In this case, $u_{(0)}^{(II)}, v_{(0)}^{(II)}$ and $v_{(1)}^{(I)}$ remain unchanged (see (3.20) and (3.25) respectively) but now $u_{(1)}^{(I)}$ has an additional term due to the presence of the vortex (2.4),

$$u_{(1)}^{(I)} = \frac{1}{\pi} \oint_{-\infty}^{\infty} \frac{H(X', t)[\partial H(X', t)/\partial X']}{(X' - X)} dX' + \frac{\tilde{\Gamma}}{\pi} \left[\frac{Y_v}{(X - X_v)^2 + Y_v^2} \right] \quad (3.29)$$

where $\tilde{\Gamma} = O(1)$ and $y = O(1)$. Evaluating the velocity field at the position of the vortex ($X = X_v, \epsilon y = Y_v$), we find that $(u_v, v_v) \sim O(\epsilon)$.

3.1.3. Case III: $\tilde{\Gamma} = O(1/\epsilon)$ and $y_v = O(1/\epsilon)$

When the vortex is strong, $\tilde{\Gamma} = O(1/\epsilon)$, the vortex contributes to the velocity field for $y = O(1)$ at leading order (2.4). If we introduce $\Gamma_0 = \epsilon \tilde{\Gamma} = O(1)$ we obtain

$$\left. \begin{aligned} u_{(0)}^{(I)} &= (H(X, t) - y) + \frac{\Gamma_0}{\pi} \left[\frac{Y_v}{(X - X_v)^2 + Y_v^2} \right], \\ v_{(0)}^{(I)} &= 0, \quad u_{(0)}^{(II)} = \frac{\Gamma_0}{\pi} \left[\frac{Y_v}{(X - X_v)^2 + Y_v^2} \right], \quad v_{(0)}^{(II)} = 0 \end{aligned} \right\} \quad (3.30)$$

and

$$\left. \begin{aligned} u_{(1)}^{(I)} &= \frac{1}{\pi} \oint_{-\infty}^{\infty} \frac{H(X', t)[\partial H(X', t)/\partial X']}{(X' - X)} dX', \\ v_{(1)}^{(I)} &= -y \frac{\partial H(X, t)}{\partial X} + \frac{2\Gamma_0}{\pi} \frac{y Y_v (X - X_v)}{((X - X_v)^2 + Y_v^2)^2}. \end{aligned} \right\} \quad (3.31)$$

Note that from (2.4) the velocity at the vortex (X_v, Y_v) is $u_{v(0)} = \Gamma_0/(4\pi Y_v)$ and $v_v = O(\epsilon)$.

3.2. The evolution of the interface

In this subsection, we use the velocity field determined in the last subsection to derive the equation governing the evolution of the interface for the three limiting cases examined. Substituting the velocity field at the interface into the kinematic condition (3.10) for cases I, II and III respectively, we obtain

$$\frac{\partial H}{\partial T} + H \frac{\partial H}{\partial X} + \frac{\partial H}{\partial X} \begin{cases} 0 \\ 0 \\ \frac{\Gamma_0}{\pi} \frac{Y_v}{Y_v^2 + (X - X_v)^2} \end{cases} = \begin{cases} 0 \\ 0 \\ \frac{2\Gamma_0}{\pi} \frac{Y_v(X - X_v)}{((X - X_v)^2 + Y_v^2)^2} H \end{cases} \quad (3.32)$$

where we have introduced the slow time variable, $T = \epsilon t$. The above results show that the vortex velocity induced by the layer is $O(\epsilon)$ and that induced by its image is equal to $c_v = \epsilon \tilde{\Gamma} / (4\pi Y_v)$. The velocity of the vortex is $O(1)$ only for the case $\tilde{\Gamma} = O(1/\epsilon)$. In this case, the horizontal velocity is constant and $c_v = \Gamma_0 / (4\pi Y_v)$. Moreover, the vertical displacement of the vortex is small relative to its initial height. Hence to leading order, $Y_v(t) \sim Y_v(0) = d$ where d is a constant. In the subsections to follow, we study different cases of the kinematic condition for various scalings of $H(X, t)$ and $\tilde{\Gamma}$ that exhibit a variety of phenomena including rapid growth, steepening of the interface, propagation of waves and which suggest cases to study numerically where ejection of vorticity may occur.

3.3. The linear evolution of the interface

We consider different limits of the kinematic equation where $\tilde{\Gamma}$ and $H(X, t)$ are such that the governing equation for the interface is linear.

3.3.1. Small-amplitude disturbances under a weak forcing

We assume the effect of the vortex on the interface is weak, $\tilde{\Gamma} = O(1)$, and the disturbance to the interface is small,

$$H(X, T) = 1 + \epsilon \eta(X, T). \quad (3.33)$$

The kinematic equation (3.32) then reduces to

$$\frac{\partial \eta}{\partial T} + \frac{\partial \eta}{\partial X} = \frac{2\tilde{\Gamma}d}{\pi} \frac{X}{(X^2 + d^2)^2}. \quad (3.34)$$

This has solutions of the form

$$\eta(X, T) = \frac{\tilde{\Gamma}d}{\pi} \left(\frac{1}{(X - T)^2 + d^2} - \frac{1}{(X^2 + d^2)} \right) \quad (3.35)$$

where the first term represents a travelling wave propagating downstream with constant speed and the second term corresponds to the steady solution associated with the point vortex. Note this is the long-wave limit of the general linear theory solution obtained in Atassi *et al.* (1997). Substituting this solution into (2.5) and taking the limit as $T \rightarrow \infty$ we see that the vertical displacement of the vortex asymptotes to the height

$$Y_v = d - \epsilon \frac{\tilde{\Gamma}}{2\pi d} \quad (3.36)$$

and that the terminal state of the system is a steady state.

3.3.2. The initial growth of disturbances

We consider the case where a small, initial disturbance is forced by a strong vortex ($\tilde{\Gamma} = O(1/\epsilon)$). For time $t = O(1)$, disturbances to the interface are small and

$$H(X, t) = 1 + \epsilon\eta(X, t). \quad (3.37)$$

The kinematic equation becomes

$$\frac{\partial\eta}{\partial t} = \frac{2\Gamma_0 d}{\pi} \frac{X}{(X^2 + d^2)^2}. \quad (3.38)$$

This equation has the solution

$$\eta(X, t) = \eta_0(X) + \frac{2\Gamma_0 d}{\pi} \frac{Xt}{(X^2 + d^2)^2}. \quad (3.39)$$

From (3.39) we can see that the expansion in equation (3.37) is not uniformly valid for $t \gg 1$ because disturbances to the interface become large. However, this solution indicates that for $t = O(1)$, the interface is going to grow linearly with time due to the forcing of the vortex and the rate of this growth is proportional to the strength of the vortex. The solution is antisymmetric in X implying that when $\Gamma_0 > 0$ ($\Gamma_0 < 0$) the interface upstream of the vortex intrudes into the wall layer (irrotational flow) and downstream the interface intrudes into the irrotational flow (wall layer). This solution corresponds to the initial stage of the vortex-induced ejection of vorticity from the thin layer to the irrotational flow and gives the initial growth of the interface for any vortex whose circulation scales like $O(1/\epsilon)$ or stronger, i.e. we can always scale t and H such that the first and fourth terms balance in (equation (3.32)) and obtain equation (3.38). When the vortex is stronger, only the timescale of the growth is faster.

The effect of this growing disturbance on the vertical vortex displacement may be calculated by substituting into equation (2.5). This yields

$$Y_v(t) = d - \frac{\epsilon\Gamma_0}{8\pi d^3} t^2. \quad (3.40)$$

This solution indicates that as the disturbance grows linearly in time the vertical displacement of the vortex from its initial position is proportional to time squared and thus implies that the expansion for the leading-order position of the vortex breaks down for $t = O(1/\epsilon^{1/2})$.

3.3.3. The effect of a strong vortex on finite-amplitude disturbances

We consider a strong vortex acting on finite-amplitude disturbances. This case corresponds to a second stage in the vortex-induced deformation of the interface where the first stage was characterized in the previous subsection and corresponded to linear growth in time. The strength of the vortex is assumed large such that the velocity it induces dominates the evolution of the interface. For this to occur, we choose $\tilde{\Gamma} = \Gamma_0/\epsilon^2$. In this case, the horizontal velocity of the vortex at leading order is due to the effect of the wall and we can write $X_v = C_v t$ where $C_v = \epsilon c_v = \Gamma_0/(4\pi d)$. Under these conditions, the evolution equation for the interface (3.32) becomes

$$\frac{\partial H}{\partial t} + \frac{\Gamma_0 d}{\pi((X - C_v t)^2 + d^2)} \frac{\partial H}{\partial X} = \frac{2\Gamma_0 d(X - C_v t)H}{\pi((X - C_v t)^2 + d^2)^2}. \quad (3.41)$$

We choose a reference frame moving with the vortex and introduce the variable $\xi = X - C_v t$. Substituting into (3.41) yields,

$$\frac{\partial H}{\partial t} + c(\xi) \frac{\partial H}{\partial \xi} = \frac{(2\Gamma_0 d)\xi H}{\pi(\xi^2 + d^2)^2}, \quad (3.42)$$

where $c(\xi) = C_v(3d^2 - \xi^2)/(\xi^2 + d^2)$. The function $c(\xi)$ has two zeros at the points

$$\xi^\pm = \pm\sqrt{3}d. \quad (3.43)$$

The two points ξ^\pm correspond to points along the characteristics which are stationary. When $\Gamma_0 > 0$ ($\Gamma_0 < 0$) the points on the interface upstream (downstream) of ξ^- (ξ^+) and downstream (upstream) of ξ^+ (ξ^-) are moving upstream (downstream) relative to the vortex whereas for $\xi^- < \xi < \xi^+$ the points are moving downstream (upstream). In order to satisfy conservation of mass in the neighbourhood of these two stationary points we expect the interface to grow (decay) rapidly near ξ^+ (ξ^-) and near ξ^- (ξ^+) to decay (grow).

From equation (3.42), we first consider the equation for the characteristics

$$-C_v dt = \frac{(\xi^2 + d^2)d\xi}{(\xi + \sqrt{3}d)(\xi - \sqrt{3}d)} \quad (3.44)$$

subject to the initial condition

$$\xi = \xi_0 \quad \text{at} \quad t = 0. \quad (3.45)$$

Solving this initial value problem, we obtain

$$t = -\frac{1}{C_v} \left\{ (\xi - \xi_0) + \frac{2d}{\sqrt{3}} \left[\ln \left| \left(\frac{\xi - \sqrt{3}d}{\xi + \sqrt{3}d} \right) \left(\frac{\xi_0 + \sqrt{3}d}{\xi_0 - \sqrt{3}d} \right) \right| \right] \right\} \quad (3.46)$$

or

$$\frac{\xi - \sqrt{3}d}{\xi + \sqrt{3}d} e^{(\sqrt{3}/2d)\xi_0} = \lambda e^{-(\sqrt{3}C_v/2d)t} \quad (3.47)$$

where $\lambda = (\xi_0 - \sqrt{3}d)/(\xi_0 + \sqrt{3}d)e^{\sqrt{3}/(2d)\xi_0}$. The characteristics are plotted in the (ξ, t) -plane in figure 3. Two asymptotes lie at $\xi^\pm = \pm\sqrt{3}d$ which are the stationary points in the flow. In figure 3(a), d and C_v are taken to be one for simplicity. The points which initially lie between the two stationary points are drawn toward the downstream stationary point, $\xi^+ = \sqrt{3}d$. The velocity of the points reaches a maximum directly below the vortex at $\xi = 0$ and then decreases to zero as we approach ξ^+ . Thus, even though points are converging towards the second stationary point, ξ_+ , their velocity goes to zero as they approach it and the characteristics do not cross in finite time. Points which are initially downstream of ξ^+ move upstream and slowly approach it whereas points which are initially upstream of ξ^- continue to propagate upstream and hence away from ξ^- .

We now consider the equation for the interface evolution,

$$-\frac{8\xi d^2}{(\xi^2 + d^2)(\xi + \sqrt{3}d)(\xi - \sqrt{3}d)} d\xi = \frac{dH}{H}. \quad (3.48)$$

Integrating equation (3.48), we obtain

$$H(\xi, t) = H(\xi_0, 0) \frac{(\xi^2 + d^2)(\xi_0^2 - 3d^2)}{(\xi_0^2 + d^2)(\xi^2 - 3d^2)}. \quad (3.49)$$

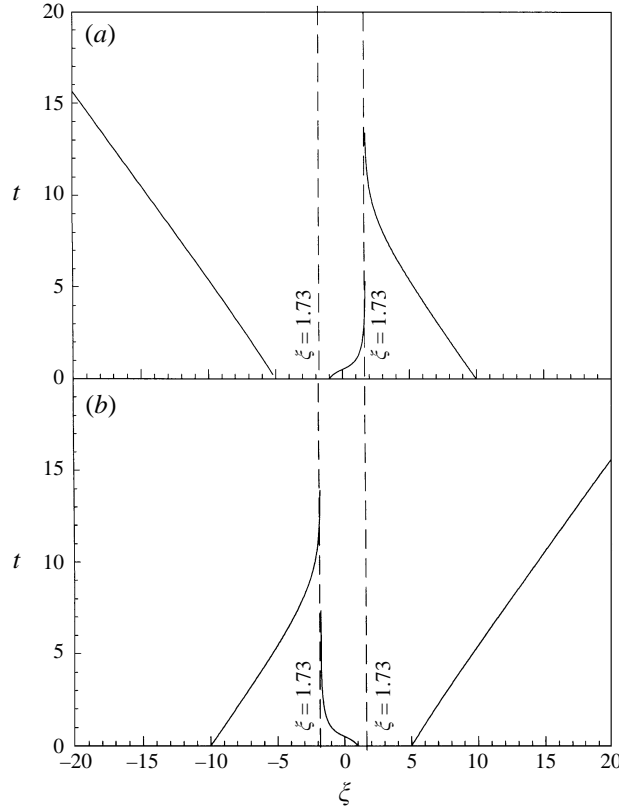


FIGURE 3. (a) The characteristics in ξ, t space for different initial locations, $\xi_0 = -5, -1, 10$ where d and c_v were chosen to be 1. Note that as time increases, disturbances propagate towards the asymptote $\xi^+ = 1.73$ for $\xi > \xi^-$ and away from the asymptote $\xi^- = -1.73$ for $\xi < \xi^+$. (b) The characteristics in ξ, t space for different initial locations, $\xi_0 = 5, 1, -10$ where $d = 1$ and $c_v = -1$. As time increases, disturbances propagate towards the asymptote $\xi^- = -1.73$ for $\xi > \xi^-$ and away from the asymptote $\xi^+ = 1.73$ for $\xi < \xi^-$.

Note that equations (3.46) and (3.49) give a parametric representation of the solution (t, H) in terms of (ξ, ξ_0) . Also note that for $\Gamma_0 > 0$ ($C_v > 0$) and $-\sqrt{3}d < \xi_0 < \sqrt{3}d$, both t and H increase monotonically with ξ . As $\xi \rightarrow \sqrt{3}d$, t and H become large. When $\xi_0 > \sqrt{3}d$, both t and H will increase as ξ decreases and become large as $\xi \rightarrow \sqrt{3}d$. Using (3.47) the asymptotic behaviour (for large t) of H in terms of t is given by

$$H(\xi^+, t) \sim \frac{H_0(\xi_0, 0)}{3} \left[\frac{(\xi_0 + \sqrt{3}d)^2}{(\xi_0^2 + d^2)} \right] e^{\sqrt{3}/(2d)[C_v t + (\sqrt{3}d - \xi_0)]}. \quad (3.50)$$

Thus for $\Gamma_0 > 0$, exponential growth occurs near $\xi = \sqrt{3}d$ in the interface height. This exponential growth is the flow response to the streamwise compression that occurs at the stationary point, ξ^+ . This solution implies that the interface will grow rapidly near ξ^+ and that nonlinear, short-scale and unsteady interaction effects between the vortex and the interface will modify the next stage of the interface evolution. Furthermore, (3.50) indicates that the timescale for the growth of the disturbance scales like d^2/Γ in this stage. This is the timescale associated with points traversing a circle of radius

d around the vortex and is consistent with the assumption that the dynamics of the interface evolution are dominated by the influence of the vortex.

When $\xi_0 < -\sqrt{3}d$ and $\Gamma_0 > 0$, we have a stable solution which for large t tends to

$$H(\xi_0, t) = H(\xi_0, 0) \frac{(\xi_0^2 - 3d^2)}{\xi_0^2 + d^2}. \quad (3.51)$$

On the other hand for $\Gamma_0 < 0$ ($C_v < 0$), if we examine (3.42) we see that the solutions to (t, H) are the same as those for $\Gamma_0 > 0$ but with t being changed to $-t$ and H to $-H$. Thus the problem exhibits time reversal symmetry. As will be seen in the results of the numerical computations as well as the nonlinear analysis in the next section, the symmetric behaviour for $\pm\Gamma_0$ is a result of the linearity. Nonlinear results clearly show a more unstable solution for $\Gamma_0 < 0$.

The results of this limiting case are in accordance with the boundary layer model of Doligalski & Walker (1984). They studied the vortex-induced separation of flow from a viscous boundary layer by solving the boundary layer equations and showed that a vortex induces an adverse pressure gradient that results in the eruption of boundary layer fluid away from the wall. Furthermore, the location of the erupting fluid occurred near the ‘outflow’ stagnation point which corresponds to $\xi^+ = \sqrt{3}d$. Thus, *the initial mechanism for ejection of vortical flow into the outer layer is the same.*

3.4. The nonlinear evolution of the interface

In this subsection, we consider two cases of equation (3.32) for the evolution of the interface. In the first case, the effect of the vortex is negligible and so the self-interaction of the layer acts alone. In the second case, the self-interaction of the layer is balanced by the effect of the vortex.

3.4.1. Finite-amplitude disturbances not influenced by the vortex

We consider the limit where $\tilde{\Gamma} \sim o(1/\epsilon)$ and $H(X, T)$ is $O(1)$. Applying (3.32), the equation governing the evolution of the interface then becomes

$$\frac{\partial H}{\partial T} + H \frac{\partial H}{\partial X} = 0. \quad (3.52)$$

This result was first derived by Stern & Pratt (1985) who were studying the evolution of a thin, unforced layer of uniform vorticity. The solution of this equation is

$$H(X, T) = H_0(X - HT) \quad (3.53)$$

where $H_0 = H(X, 0)$ is the initial shape of the interface. The solution indicates that the higher portions of the interface propagate faster than the lower parts resulting in the formation of a vorticity front. Moreover, this implies that steepening will occur on the downstream side of the disturbance and breaking will occur at

$$T_b = -\min \left[\frac{1}{H'_0(X - HT)} \right]. \quad (3.54)$$

This result has also been shown to occur for more general distributions of vorticity (Jimenez & Orlandi 1993). Before the vorticity front overturns and becomes multi-valued, nonlinear short-wave interactions become important and equation (3.52) breaks down. However, since this system is dispersive (Rayleigh 1887), we expect dispersion to counteract the steepening effect of the nonlinearity. In particular, if we further assume that the disturbances to the layer are small and the vortex has a very weak influence on the interface, $\tilde{\Gamma} \sim o(1)$, then a weakly nonlinear analysis

can be done where steepening effects and dispersion may balance each other to result in a wave of permanent form. The equation which governs this balance is the Benjamin–Ono equation (Stern & Pratt 1985; Atassi 1997),

$$\frac{\partial \eta}{\partial \tilde{T}} + \eta \frac{\partial \eta}{\partial \tilde{X}} - \frac{1}{2\pi} \int_{-\infty}^{\infty} e^{-ik\tilde{X}} |k| \int_{-\infty}^{\infty} \frac{\partial \eta}{\partial X'} e^{ikX'} dX' dk = 0 \quad (3.55)$$

where $\tilde{T} = \epsilon^2 t$ and $\tilde{X} = X - T$. The integral term in (3.55) represents the dispersive effect of the irrotational flow on the shear layer. This equation and its solitary wave solutions have also been both observed and shown to exist in two-dimensional, transitioning boundary layers (Kachanov, Ryzhov & Smith 1993) and in stratified flows of large depth (Benjamin 1967; Davis & Acrivos 1967). Equation (3.55) has solutions of the form (Benjamin 1967)

$$\eta(\tilde{X}, \tilde{T}) = \frac{1}{1 + \tilde{X}^2}. \quad (3.56)$$

Note that this solution also has the same form as the linear long-wave limit solution (3.35). Note also that the integral term in (3.55) which represents dispersive effects is directly proportional to the slope of the interface implying that dispersive effects become more important as the interface steepens.

Finally, when no vortex is present, weakly nonlinear effects have been shown to be important for the evolution of slowly modulated wave packets (Balagondar, Maslowe & Melkonian 1987; Pullin *et al.* 1989). The nonlinear Schrödinger equation describes this evolution and Pullin *et al.* (1989) have suggested that instability associated with the NLS equation may explain the focusing of vorticity into thin filaments.

3.4.2. Balance between the nonlinear self-interaction of the layer and the vortex

In § 3.3.3, we showed that when the vortex dominates the flow growing disturbances result in the neighbourhood of the unstable stationary point. Furthermore, the vortex-dominated flow is antisymmetric with respect to the orientation of the vortex, i.e. $\Gamma_{(0)} \rightarrow -\Gamma_{(0)}$, $t \rightarrow -t$ implies $(u, v) \rightarrow -(u, v)$. In this subsection, we consider the complete nonlinear evolution equation (3.32) to investigate the effect that the nonlinear self-interaction of the interface has on the vortex-induced ejection described in the previous subsection.

The equation governing the evolution of the interface is

$$\frac{\partial H}{\partial T} + c(H, \xi) \frac{\partial H}{\partial \xi} = \frac{(2\Gamma_0 d)\xi H}{\pi(\xi^2 + d^2)^2} \quad (3.57)$$

where $\xi = X - c_v T$ and where

$$c(H, \xi) = (H - c_v) + \frac{\Gamma_0 d}{\pi(\xi^2 + d^2)}. \quad (3.58)$$

The wave speed along the characteristics is stationary if

$$\xi^{\pm} = d \left(\frac{3\Gamma_0 + 4\pi d H}{\Gamma_0 - 4\pi d H} \right)^{1/2}. \quad (3.59)$$

For this to occur, the following conditions must be satisfied:

$$\left. \begin{aligned} H(\xi, T) &< \frac{\Gamma_0}{4\pi d} \quad \text{for } \Gamma_0 > 0 \\ H(\xi, T) &< \frac{3|\Gamma_0|}{4\pi d} \quad \text{for } \Gamma_0 < 0. \end{aligned} \right\} \quad (3.60)$$

Note that the condition for $\Gamma_0 > 0$ is much more restrictive and implies that the horizontal velocity of the vortex must be greater than the horizontal velocity of the unforced (3.52) layer. Since instability is associated with the existence of stationary points, $\Gamma_0 < 0$ will lead to instabilities for vortices which are three times weaker than vortices for which $\Gamma_0 > 0$.

The term $c(H, \xi)$ corresponds to the horizontal velocity of the interface disturbance. The nonlinear self-interaction term implies that higher points will propagate faster than lower points resulting in the formation of a shock on the downstream face of the disturbance. If $\Gamma_0 > 0$, the nonlinear term adds to the horizontal velocity of the interfacial disturbances and we expect the disturbances to propagate downstream with a velocity which is much higher than that of the vortex. Conversely, if $\Gamma_0 < 0$ the nonlinear term reduces the horizontal velocity of the interfacial disturbances and hence the interface will undergo a much more sustained interaction with the vortex.

As in §3.3.3, solutions to (3.57) may be determined in the neighbourhood of the stationary points, ξ^\pm , and it is found that near $\xi^+(\xi^-)$ and $\Gamma_0 > 0$ disturbances will grow (decay). Similarly, when $\Gamma_0 < 0$ disturbances will grow (decay) near $\xi^-(\xi^+)$. However, in this case equation (3.60) shows that stationary points can more easily exist when $\Gamma_0 < 0$ than $\Gamma_0 > 0$. Physically, this suggests that when the horizontal velocity induced by the vortex is counter to that of the layer a back flow in a reference frame moving with the vortex is more likely to occur and which results in the ejection of vorticity into the irrotational flow.

Finally, the horizontal velocity due to the effect of the vortex decreases as one moves away from the vortex. As a result, for a disturbance downstream of the vortex ($\tilde{T} > 0$) we expect steepening to occur on the upstream face of the disturbance. Hence, the steepening effect of the point vortex and the layer may act in opposite directions suggesting that under the right conditions the forcing and the self-interaction may balance, resulting in the propagation of a solitary wave. This possibility is suggested by rewriting equation (3.57) in conservation form,

$$\frac{\partial H}{\partial T} + \frac{\partial}{\partial \xi} \left[H^2/2 + \frac{\Gamma_0 dH}{\pi(\xi^2 + d^2)} - c_v H \right] = 0. \quad (3.61)$$

4. Numerical method

The system of equations (2.3)–(2.4) is solved using the Lagrangian method of contour dynamics (Zabusky *et al.* 1979), which tracks the deformation of the interface. Equations (2.3) and (2.4) are spatially integrated by applying the trapezoidal rule. The Lagrangian points which comprise the interface,

$$\frac{dx}{dt} = u, \quad (4.1)$$

$$\frac{dy}{dt} = v \quad (4.2)$$

and the point vortex

$$\frac{dx_v}{dt} = u_v, \quad (4.3)$$

$$\frac{dy_v}{dt} = v_v \quad (4.4)$$

are integrated temporally using a second-order Adams–Bashforth scheme. To save computation time the numerical integration is limited to the perturbed part of the interface, i.e. disturbances which depart from the height of the unperturbed interface by more than 10^{-5} . An analytic solution to (2.2) is used for the unperturbed layer, i.e. the region $(-\infty, \infty)U[0, 1]$. The spatial domain was adjusted such that when an endpoint exceeded the height of the unperturbed interface by more than 10^{-5} , a point was added to the end of the domain.

We choose, in §4.3, $y_v(0) = 10$ and a large computational domain initially extending from $[-100, 100]$. To efficiently collocate the points we initially distribute them non-uniformly where the density of points is a maximum directly below the vortex, $x = 0$. It was found that in the cases considered, the velocity field advected the Lagrangian points towards regions of large velocity variation. Using this set of non-uniformly distributed points, we were able to resolve relatively small scales without resorting to an adaptive node adjustment scheme. To this end, we introduce a weight function, $W(x)$, such that

$$\sum_{i=0}^N W(x_i)\Delta x = (N + 1)\Delta x = \text{the length of the computational domain} \quad (4.5)$$

where $(N + 1)$ corresponds to the number of points and Δx is a uniform distance between points determined by the ratio of the length of the computational domain to the number of points in the domain. The weighting function is a quadratic polynomial of the form

$$W(x_i) = \alpha_0 x_i^2 + \alpha_1 \quad (4.6)$$

where α_0 and α_1 are constants and x_i correspond to equally spaced points on the interface. Furthermore, we impose the smallest spacing between the points at $x = 0$, implying

$$\alpha_1 = W(0) \quad (4.7)$$

where $W(0)$ is a chosen parameter. Substituting (4.6) and (4.7) into (4.5) and solving we obtain

$$\alpha_0 = \frac{(N + 1)(1 - W(0))\Delta x}{\sum_{i=0}^N x_i^2} + W(0). \quad (4.8)$$

For the numerical cases to be studied, $W(0) = 1/10$.

4.1. Numerical results

In this section, we present the results of the contour dynamics simulations. The range of magnitude of the vortex strength and height is estimated from the following two examples. If the vortex is shed from an airfoil and lies outside a boundary layer of thickness δ , then assuming $H_\infty = \delta/5$, we find $|\tilde{\Gamma}| \sim 2.5c_L(c/\delta) = 10\text{--}40$, where c_L is the lift coefficient and c is the airfoil chord. For a vortex lying in the outer layer of a turbulent boundary layer, $\tilde{\Gamma} = O(U\delta)$. This gives a range, $|\tilde{\Gamma}| \sim 2\text{--}8$.

$\tilde{\Gamma}$	$y_v(t=0)$	$H(x, t=0)$	c_v
± 5	10	1	± 0.04
± 10	10	1	± 0.08
± 20	10	1	± 0.16
± 40	10	1	± 0.32

TABLE 1. Selected parameters for the eight cases. Recall $c_v = \tilde{\Gamma}/(4\pi y_v(0))$ is the initial horizontal velocity induced by the image vortex. Note that the cases where $\tilde{\Gamma} > 0$ correspond to situations where the vortex is in phase with vorticity in the layer whereas when $\tilde{\Gamma} < 0$ the vortex is 180° out of phase with the vorticity in the layer.

The cases studied can be divided into two groups. The first group corresponds to the shed-vortex case where the vortex is far above the interface relative to the thickness of the shear layer. In this case, the thin layer theory developed in the last section is applicable for small times where the slope of the interface and the displacement of the vortex due to the layer are not too large. For larger times, these assumptions are no longer valid and the only alternative is to study these cases numerically. The second group of cases assume that the vortex lies close to the layer, i.e. within the order of the thickness of the layer. Although the theory developed in §3 does not apply for this group of cases, we investigate whether the initial qualitative behaviour is the same. For example, we examine whether the amplitude of the interfacial disturbances is larger and the unsteady interaction more sustained when the circulation of the vortex is counter to that of the layer. We also study the dynamic effects of the vortex–shear layer interaction by computing the wall pressure for several cases. As a measure of the numerical error, the results are compared with conservation of x -momentum and conservation of vorticity at each timestep.

4.1.1. Vortex of varying strength far above the shear layer

We present several plots of the time evolution of the interface between the shear layer and the potential flow region. In each case, the interface is initially flat and the vortex is placed ten layer thicknesses above the interface. The strength and direction of the circulation are varied in eight cases, shown in table 1, to (i) determine the initial conditions under which a strong interaction between the vortex and the layer takes place and results in the ejection of vorticity into the irrotational flow and (ii) compare the evolution of the interface with the theory developed in §3.

In figure 4, the deformation of the interface is shown for the cases $\tilde{\Gamma} = 5, 10, 20, 40$. In these cases, the sense of the rotation of the vortex is the same as the sense of the vorticity in the layer, i.e. $\tilde{\Gamma} > 0$. All the cases are run until $t = 50$ except for the $\tilde{\Gamma} = 40$ case which is stopped at $t = 30$ because of the formation of small scales. The vortex is off the scale of the figure. For $0 < t < 10$, the vortex deforms the interface causing a trough to form directly below the vortex. Downstream of the trough a wave propagates downstream at a speed close to one, i.e. the unperturbed horizontal velocity of the wall. In the four cases considered, the amplitude of the disturbances ranges from 0.2 to 1 with the largest corresponding to the vortex with the greatest circulation. When the interfacial disturbances are not too large ($\tilde{\Gamma} = 5, 10$), we expect the wave-like behaviour to be qualitatively similar to the linear and weakly nonlinear equations ((3.35) and (3.55)).

For the cases where $\tilde{\Gamma} = 5$ and 10 two disturbances are formed: a steady trough which remains below the vortex and a solitary wave which propagates downstream

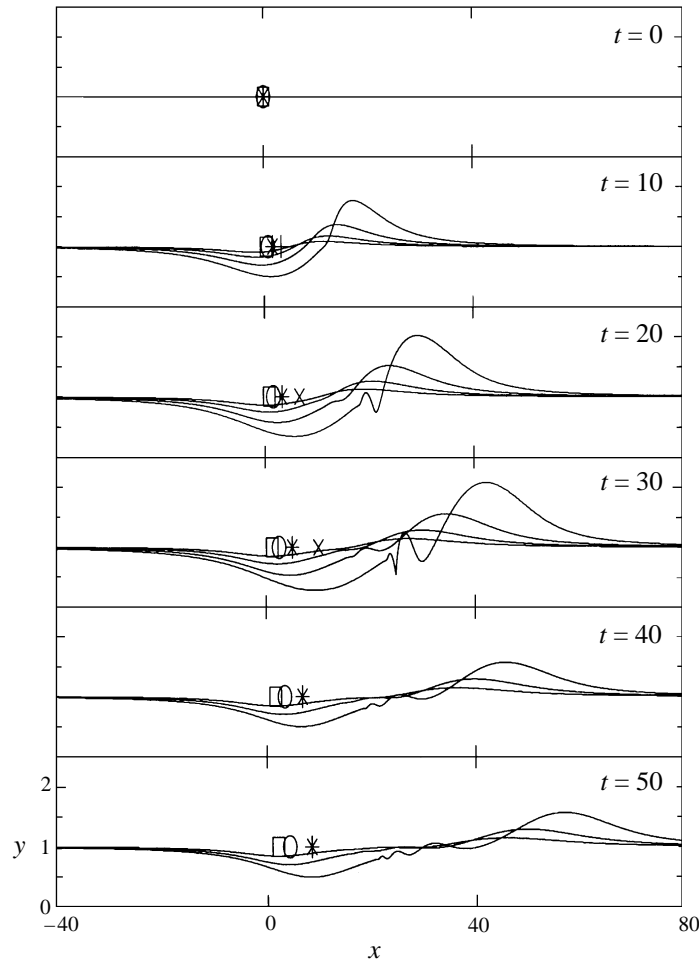


FIGURE 4. The deformation of the interface delineating the uniform vorticity layer from the irrotational flow at five different times. The circulation of the vortex is $\tilde{\Gamma} = 5, 10, 20, 40$ and its initial height is $y_v(0) = 10$. The vertical height of the vortex is outside the scale of the figure. The square, circle, asterisk and \times correspond to the x -location of the vortex for the cases $\tilde{\Gamma} = 5, 10, 20, 40$ respectively. The smallest disturbances to the interface correspond to the smallest values of $\tilde{\Gamma}$.

with a speed close to one. This is in agreement with the linear solution (3.35) which shows that a steady solution below the vortex is superposed with a solitary wave which propagates downstream with speed near one. When $\tilde{\Gamma} = 20$ and 40 the amplitude of the interfacial disturbances is larger and dispersion becomes significant as the upstream side of the wave steepens. As a result, small waves are left upstream of the main disturbance but far downstream of the vortex. Nonlinear effects modify the linear and weakly nonlinear solutions (3.35), (3.55). The dispersion which is observed is qualitatively consistent with (3.55) which shows that dispersive effects become more important when the slope of the interface steepens.

Since the amplitude of the interfacial disturbances is not too large, we also expect that the velocity induced by the deformed interface on the vortex is small since the vortex lies far above the interface (equation (3.28)). As a result, the horizontal velocity of the vortex should be approximately $c_v = \tilde{\Gamma} / (4\pi d) = 0.04, 0.08, 0.16, 0.32$ for the four

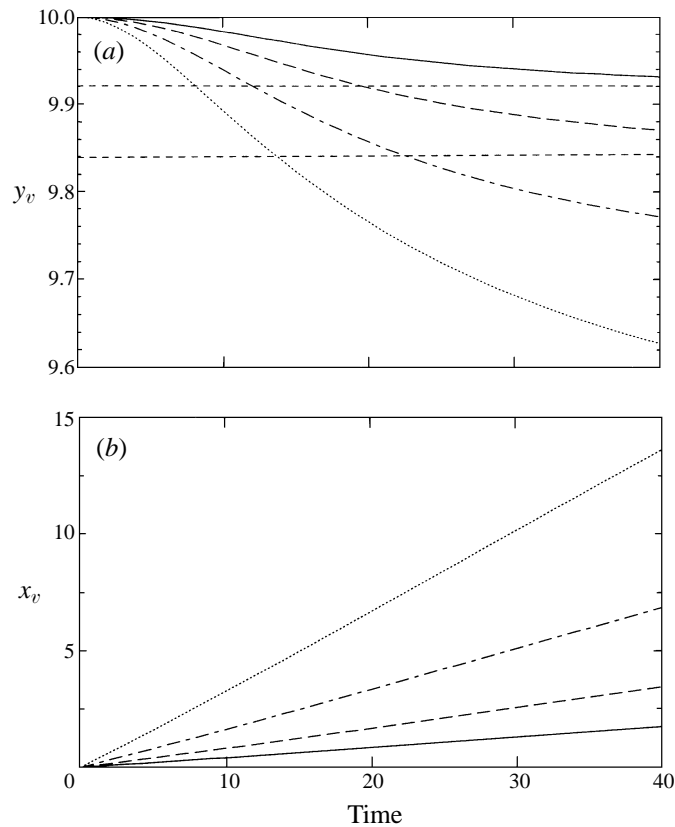


FIGURE 5. The horizontal and vertical displacement of the vortex. The circulation of the vortex is $\tilde{\Gamma} = 40$ and its initial height $y_v(0) = 10$. The solid line corresponds to $\Gamma = 5$, the dashed line $\Gamma = 10$, the dot-dashed line $\Gamma = 20$, and the dotted line $\Gamma = 40$. The long-time height predicted by the thin layer theory is indicated by the horizontal dashed lines in (a).

$\tilde{\Gamma} / (4\pi y_v(0))$	\bar{c}_v
0.04	0.04
0.08	0.08
0.16	0.17
0.32	0.34

TABLE 2. A comparison of the theoretically approximated values of c_v used in §3 and the numerical values, \bar{c}_v .

cases. This is confirmed in table 2 comparing the value $c_v = \tilde{\Gamma} / (4\pi d)$ with the average value of the numerical results shown in figure 5(b). These computations support the asymptotic analysis in §3 where the leading-order horizontal velocity was assumed to be c_v . Since the horizontal velocity of the vortex is small relative to the downstream velocity of the propagating wave, the interaction between the vortex and the interface is expected to wane for long times. The diminishing interaction can be seen in figure 5(a) where the vertical displacement of the vortex is plotted as a function of time. In all four cases, the descent of the vortex is small justifying the asymptotic expansions made in §3. Moreover, for long times the descent of the vortex slows and appears

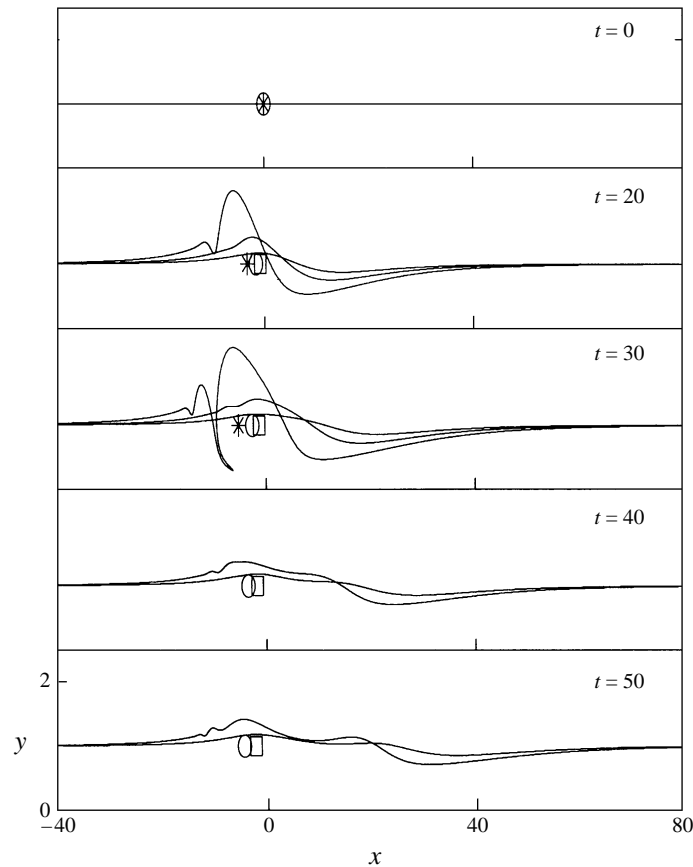


FIGURE 6. The deformation of the interface delineating the uniform vorticity layer from the irrotational flow at five different times. The circulation of the vortex is $\tilde{\Gamma} = -5, -10, -20$ and its initial height is $y_v(0) = 10$. The vertical height of the vortex is outside the scale of the figure. The square, circle and asterisk correspond to the x -location of the vortex for the cases $\tilde{\Gamma} = -5, -10, -20$ respectively.

to asymptote to an equilibrium height. For $\tilde{\Gamma} = 5$ and 10 the decreasing rate of descent of the vortex with time is most clearly seen and so we compare these cases to the asymptotic result (3.36). The analytical solution is indicated in figure 5(a) by the dashed horizontal line and corresponds to the long-time steady-state height of the vortex. For $\tilde{\Gamma} = 5$ and 10 this small-amplitude, asymptotic solution gives good agreement with the contour dynamics solution.

Figure 6 presents the deformation when $\tilde{\Gamma} = -5, -10, -20$ where the circulation of the vortex has sign opposite to the vorticity in the wall layer. All the cases are run until $t = 50$ except for the $\tilde{\Gamma} = -20$ case which is stopped at $t = 30$ because of the formation of small scales. As in the first set of cases, the amplitude of the interfacial disturbances grow with increasing $|\tilde{\Gamma}|$. However, here the amplitude of the disturbances is much larger and for the case $\tilde{\Gamma} = -20$ overturning and entrainment of irrotational flow occurs. Moreover, from $\tilde{\Gamma} = -10$ to -20 a bifurcation in behaviour occurs from wave-like disturbances to ejection of a large blob of vorticity which is overturning and entraining irrotational flow into the layer.

Figures 7 and 8 present a more detailed view of the deformation of the interface

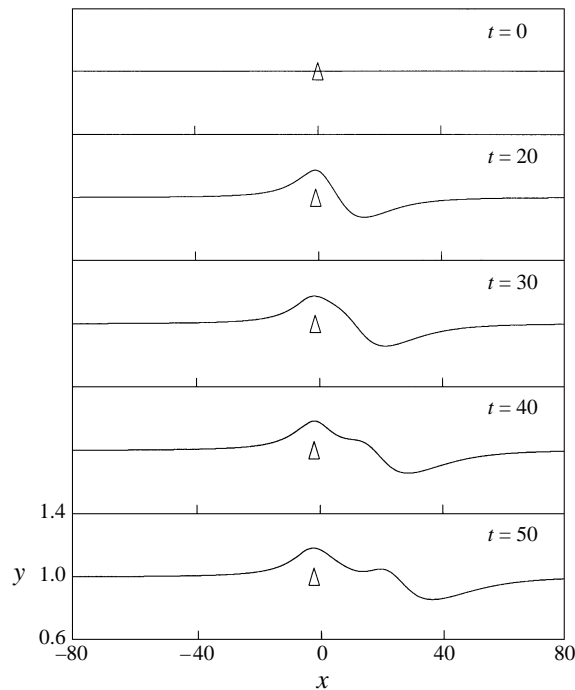
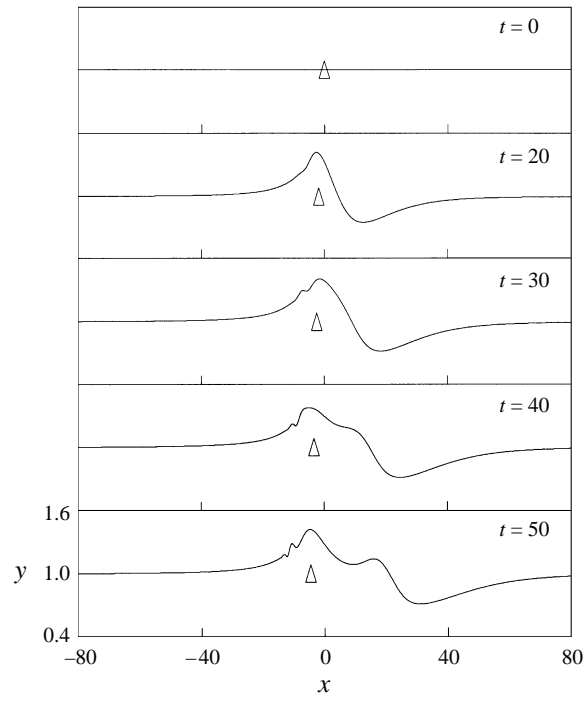
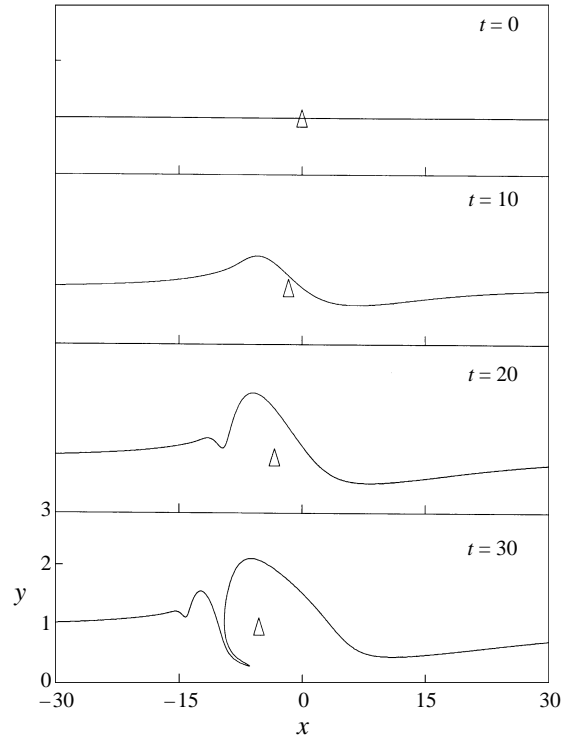


FIGURE 7. The deformation of the interface delineating the uniform vorticity layer from the irrotational flow at five different times. The circulation of the vortex is $\tilde{\Gamma} = -5$ and its initial height is $y_v(0) = 10$. The vertical height of the vortex is outside the scale of the figure. The x -location of the vortex is indicated by the upward pointing triangle.

when $\tilde{\Gamma} = -5$ and -10 . For $0 < t < 30$, the behaviour in both cases is characterized by growth and steepening of the interface directly below the vortex. For longer times a trough propagates downstream and a positive disturbance lies directly below the vortex. These solutions are qualitatively similar to (3.35) for $\tilde{\Gamma} < 0$. Moreover, the vertical ascent of the vortex to an equilibrium height (figure 11) is close to that predicted by the linear theory (3.36) and is indicated in figure 11(a) by the dashed line. When $\tilde{\Gamma} = -10$, the amplitude of the disturbance is larger (0.5) and exhibits nonlinear steepening. Eventually, small-scale dispersive waves form on the upstream face of the positive disturbance. Also note that in figure 7 the amplitude of the wave is nearly 0.3 times the initial thickness of the layer while in figure 8 it is nearly 0.6 times its initial thickness. These disturbances are larger than those shown in figure 4 where $\tilde{\Gamma} = 5$ and 10 , respectively. We also observe that the distance between the x -location of the vortex and the x -location of the disturbance is much smaller than those shown in figure 4.

In figures 9 and 10 the circulation of the vortex is $\tilde{\Gamma} = -20$ and $\tilde{\Gamma} = -40$, respectively. However, as opposed to the travelling wave-like solutions shown in figures 4, 7 and 8 we observe a bifurcation in behaviour to growing mound-like disturbances which overturn and entrain irrotational flow deep into the layer. When $\tilde{\Gamma} = -20$, the interface exhibits rapid and continuous growth until $t = 20$. After $t = 20$, the interface overturns and a narrowing crevice of irrotational flow is entrained into the layer. When $\tilde{\Gamma} = -40$, rapid growth occurs throughout the entire simulation, $0 \leq t \leq 30$. The initial growth of the shear layer has the same asymmetric form as given by equation (3.38). The narrowing finger of vorticity is then ejected far

FIGURE 8. As figure 7 but for $\tilde{\Gamma} = -10$.FIGURE 9. As figure 7 but for four different times and the circulation of the vortex is $\tilde{\Gamma} = -20$.

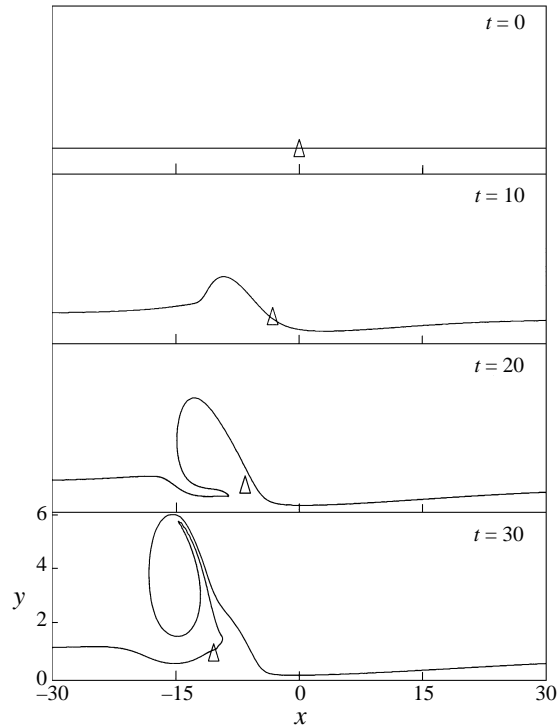


FIGURE 10. As figure 9 but for $\tilde{\Gamma} = -40$.

$\tilde{\Gamma}/(4\pi y_t(0))$	\bar{c}_v
-0.04	-0.04
-0.08	-0.08
-0.16	-0.17
-0.32	-0.34

TABLE 3. A comparison of the theoretically approximated values of c_v used in §3 and the numerical values, \bar{c}_v .

into the irrotational flow and rolls up. By $t = 30$, the disturbance has grown to an amplitude of nearly six times the initial thickness of the layer. Note that downstream of the disturbance the thickness of the layer is approximately 0.2; this illustrates that vorticity is taken from downstream of the vortex and is ejected into the irrotational flow.

Figures 11 and 12 show the horizontal and vertical displacements of the vortex for the cases $\tilde{\Gamma} = -5, -10, -20, -40$ respectively. The horizontal velocities of the vortex are nearly constant and equal to c_v in all four cases as shown in table 3. This is confirmed in the table comparing the value $c_v = \tilde{\Gamma}/(4\pi d)$ with the average value of the numerical results shown in figure 11(b). Again the similarity between c_v and \bar{c}_v support the arguments and analysis in §3. The vertical displacement of the vortex is much larger when $\tilde{\Gamma} = -40$ and its vertical velocity has not levelled off by $t = 30$ implying a strong and sustained interaction between the vortex and the layer. Also the velocity induced by the layer displaces the vortex away from the layer. As a result,

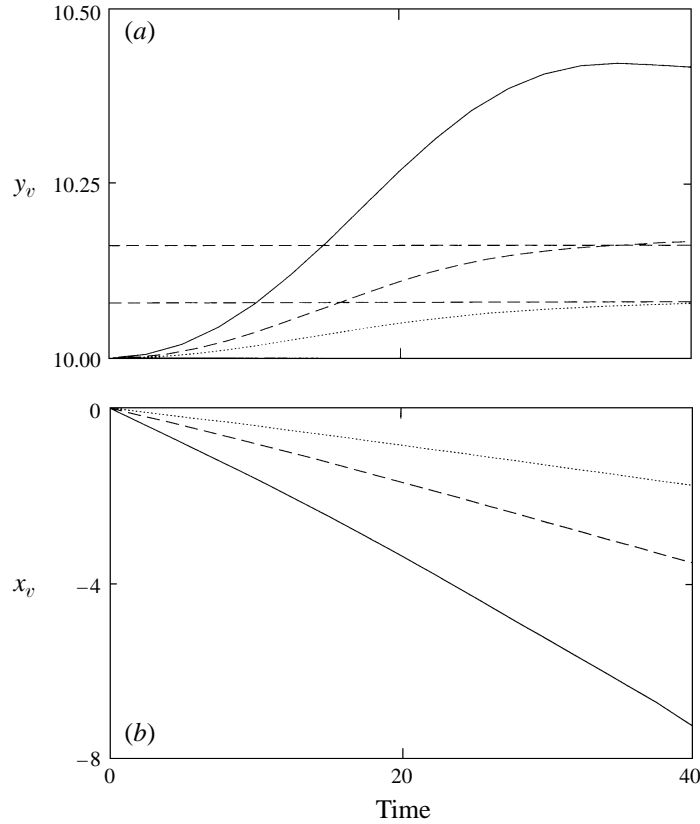


FIGURE 11. The horizontal and vertical displacement of the vortex. The circulation of the vortex is $\tilde{\Gamma} = -5, -10, -20$ and its initial height is $y_v(0) = 10$. The solid line corresponds to $\tilde{\Gamma} = -20$, the dashed line $\tilde{\Gamma} = -10$ and the dotted line $\tilde{\Gamma} = -5$. The long-time height predicted by the thin layer theory for $\tilde{\Gamma} = -5, -10$ is indicated by the horizontal dashed lines in (a).

one might then expect that the interaction should wane more quickly than the $\tilde{\Gamma} = 40$ case. However, since the horizontal velocity of the disturbance is close to that of the vortex, as is indicated by the upward pointing triangle in figure 10, the total distance between the vortex and the layer does not grow very large with time and a strong unsteady interaction is sustained. Moreover, the large bifurcation in behaviour that occurs between the $\tilde{\Gamma} > 0$ and $\tilde{\Gamma} < 0$ cases (figures 4 & 10) indicates that the sense of the vortex plays an important role in the overturning and ejection of the vorticity in the layer.

In figure 13 we present the pathlines of the vortex for the cases $\tilde{\Gamma} = 5, 10, 20, 40$ and $\tilde{\Gamma} = -5, -10, -20, -40$ where $0 \leq t \leq 30$. When $\tilde{\Gamma} > 0$, the vertical displacement of the vortex is towards the layer and the horizontal distance the vortex moves downstream by $t = 30$ is directly related to the vortex strength. However, the vortex paths are nearly the same, regardless of the vortex strength. For $\tilde{\Gamma} < 0$, the vortex is vertically displaced away from the layer and propagates upstream a horizontal distance which is proportional to the vortex strength. Despite the ascent of the vortex away from the layer for $\tilde{\Gamma} < 0$, we observe that the interaction is stronger when $\tilde{\Gamma} < 0$ than when $\tilde{\Gamma} > 0$, even though the vortex moves closer to the layer in this

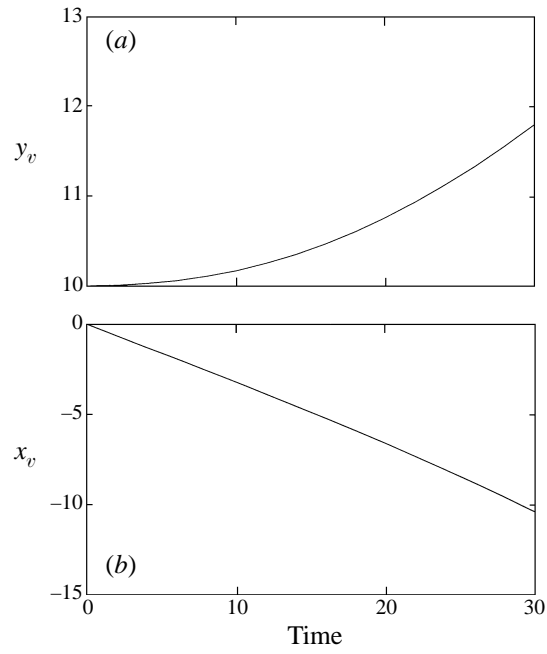


FIGURE 12. The horizontal and vertical displacement of the vortex. The circulation of the vortex is $\tilde{\Gamma} = -40$ and its initial height is $y_v(0) = 10$.

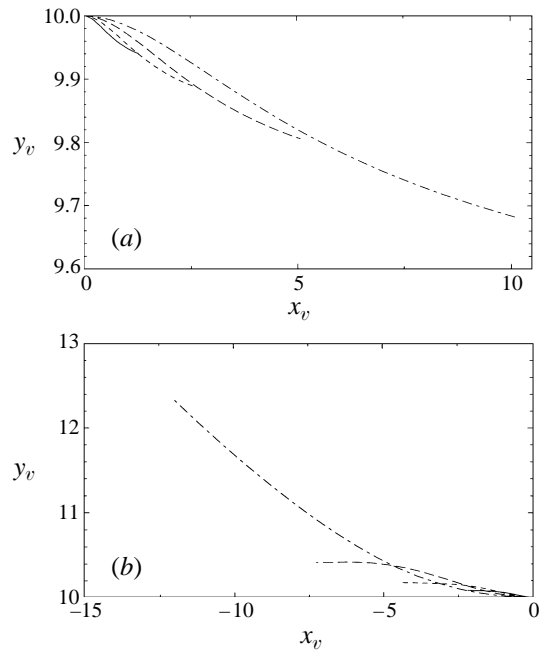


FIGURE 13. The pathlines of the vortex for $0 \leq t \leq 30$: (a) $\tilde{\Gamma} = 5, 10, 20, 40$, (b) $\tilde{\Gamma} = -5, -10, -20, -40$. The solid, dashed, long-dashed, and dot-dashed lines correspond to $\tilde{\Gamma} = \pm 5, \pm 10, \pm 20, \pm 40$ respectively.

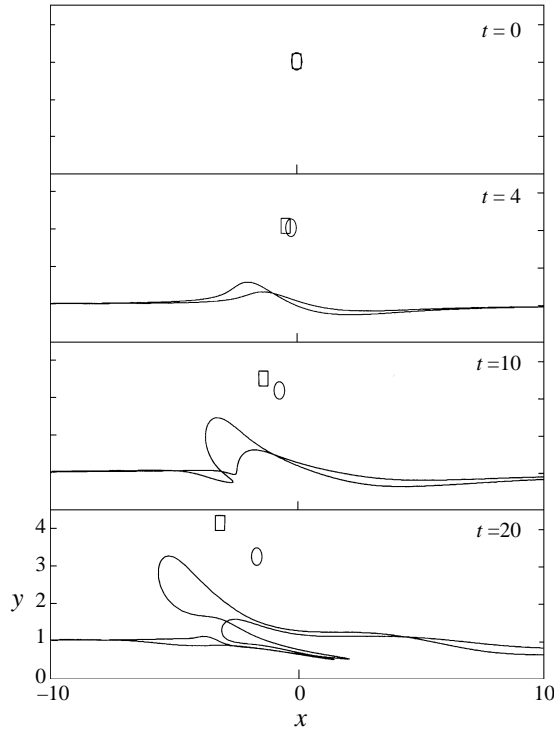


FIGURE 14. The deformation of the interface delineating the uniform vorticity layer from the irrotational flow at four different times. The circulation of the vortex is $\tilde{\Gamma} = -2, -4$ and the initial height of the vortex is $y_v(0) = 3$. The square and circle indicate the position of the vortex for the cases $\tilde{\Gamma} = -2, -4$.

case. This suggests that the vertical displacement does not significantly change the qualitative behaviour of the interaction.

4.1.2. Vortex of varying strength lying close to the thin layer

We consider three cases where the vortex is initially close to the layer, i.e. $y_v(0) = 3$, and we vary the strength and orientation of the vortex such that $\tilde{\Gamma} = -2, -4, -8$. In all three cases, the evolution of the interface is studied from $0 \leq t \leq 20$ and the interface is initially flat. We have observed in figure 13 that when $\tilde{\Gamma} < 0$ the vortex ascends from the layer and when $\tilde{\Gamma} > 0$ the vortex descends towards the layer. In spite of this, we observed that large disturbances and a strong vortex–layer interaction occur when $\tilde{\Gamma} < 0$. However, in the three cases studied in this subsection the vortex is close to the layer, so its vertical displacement may play a more important role in the evolution of the interface. We thus study these cases to see if the qualitative behaviour of the system changes significantly when the vortex is not far above the layer.

We first consider the two cases where the circulation of the vortex is opposite in sense to that of the layer. In figure 14, $\tilde{\Gamma} = -2, -4$. For $\tilde{\Gamma} = -2$, the interface initially grows to an amplitude of nearly 2. By $t = 10$, the disturbance begins to overturn and the growth then appears to slow. Once it starts to overturn, irrotational flow is entrained into the layer in a thin crevice which grows in the downstream direction. Also in figure 14, for $\tilde{\Gamma} = -4$, a larger disturbance forms and more rapid growth is observed. By $t = 10$ the disturbance has steepened and begins to overturn.

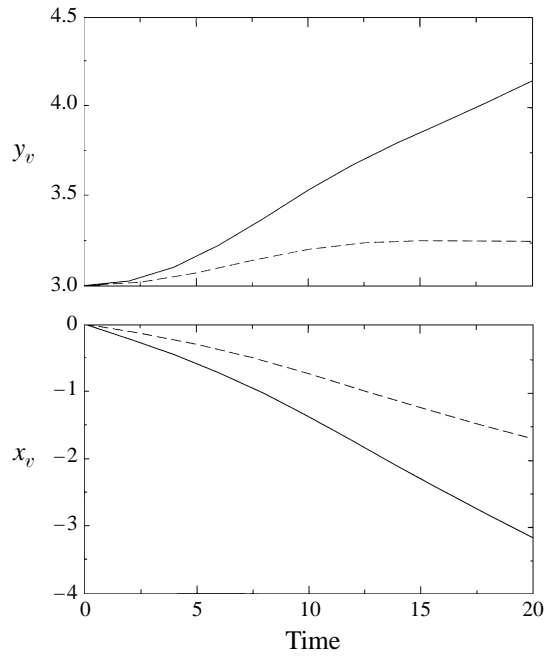


FIGURE 15. The vertical and horizontal displacement of the vortex. The solid line corresponds to the vortex with circulation $\tilde{\Gamma} = -4$, the dashed line $\tilde{\Gamma} = -2$. The initial height of the vortex is $y_v(0) = 3$.

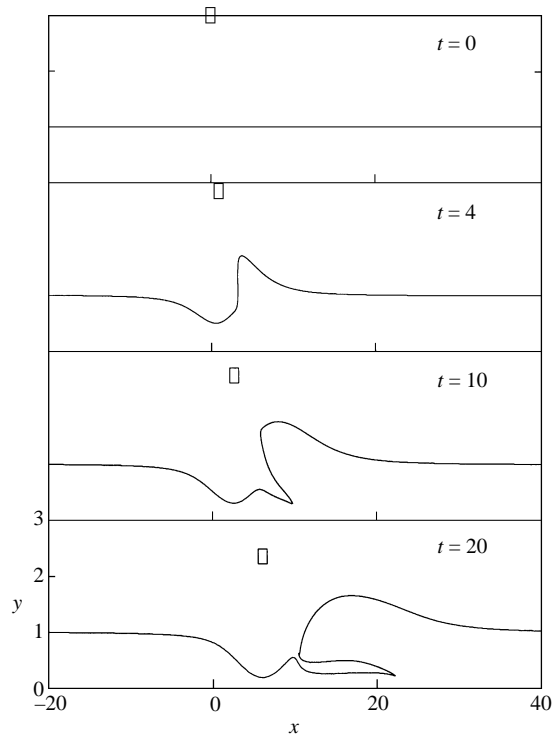


FIGURE 16. The deformation of the interface delineating the uniform vorticity layer from the irrotational flow at four different times. The circulation of the vortex is $\tilde{\Gamma} = 8$ and its initial height is $y_v(0) = 3$.

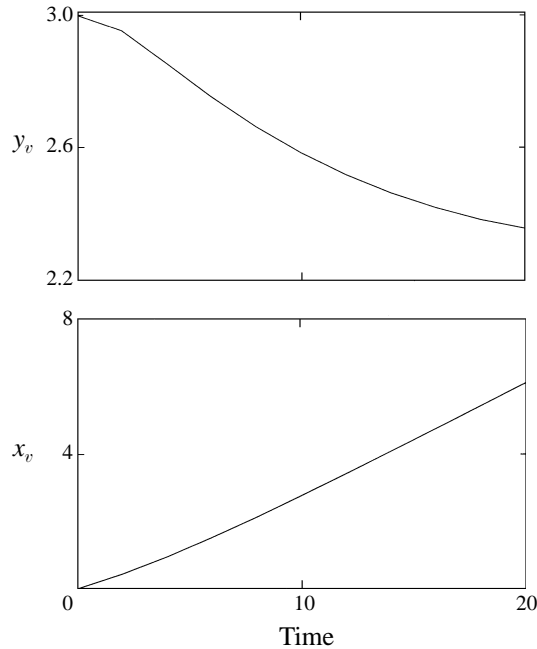


FIGURE 17. The horizontal and vertical displacement of the vortex. The circulation of the vortex is $\tilde{\Gamma} = 8$ and its initial height is $y_v(0) = 3$.

In this case the growth continues and by $t = 20$ the disturbance has been stretched into a thin finger of vorticity which extends into the irrotational flow to a height of approximately 3.2. In both cases, the vortices move away from the layer.

Figure 15 shows the displacement of the vortex for these two cases. When $\tilde{\Gamma} = -2$ we see that the interaction appears to wane around $t = 10$ as is indicated by the vertical vortex position levelling off. By $t = 20$ the vortex has ascended to a height of nearly 3.2. However, for $\tilde{\Gamma} = -4$ the interaction is stronger and although the vortex is displaced to a height of 4.2 ($t = 20$), the unsteady interaction continues to persist as is indicated by the vortex continuing to move away from the layer.

We now consider a stronger vortex but one where the circulation has the same sense as that of the layer (figure 16). In this case, a disturbance is seen to grow to an amplitude of 2 and propagate downstream. By $t = 10$ the disturbance steepens and begins to roll up and entrain irrotational fluid. From figure 17, we see by the vertical displacement of the vortex that the interaction of the vortex with the interface appears to wane to a small extent by $t = 10$. This occurs despite the descent of the vortex toward the layer which by $t = 20$ is at $y_v = 2.2$. However, the distance between the x -location of the vortex and the primary interfacial disturbance is increasing with time as is evident in figure 16. Thus, even though the vortex descends towards the interface, the total distance from the interfacial disturbance grows with time.

Both positive and negative vortices near the layer can result in rollup and entrain irrotational fluid. However, the interaction with a negative vortex is stronger. In this case the layer deforms more even though the magnitude of the circulations of the vortices in figure 14 are smaller than the circulation of the vortex in figure 15 and the negative vortices mover upward, away from the layer.

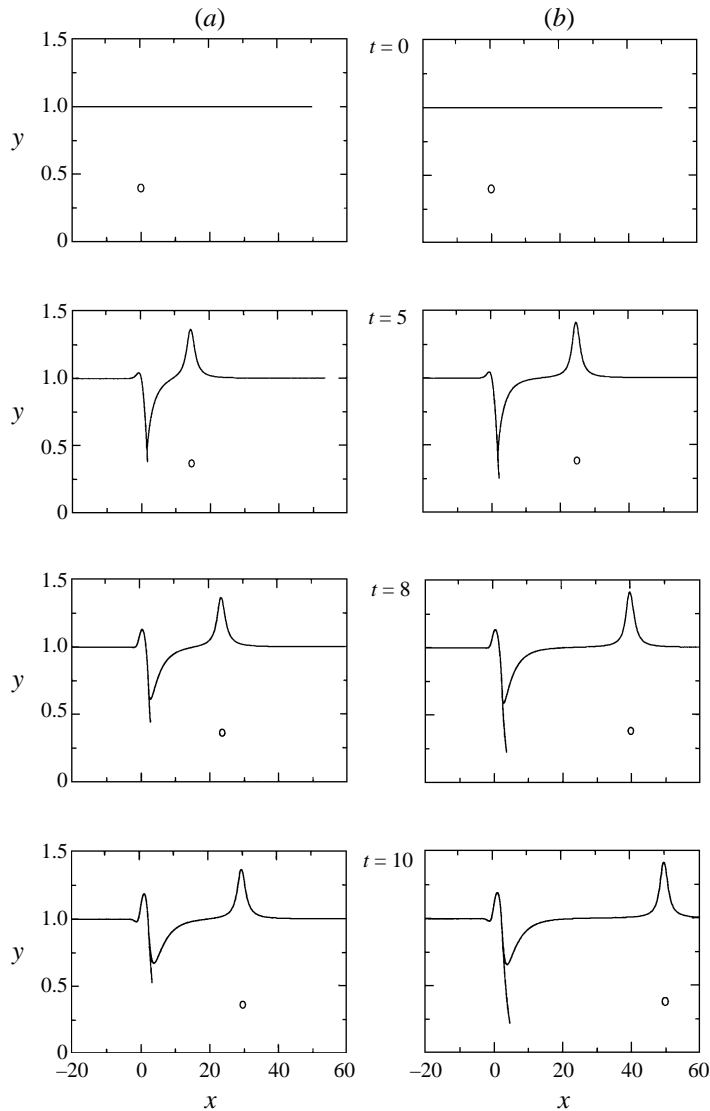


FIGURE 18. The deformation of the interface for $t = 0, 5, 8, 10$. In column (a), $\tilde{\Gamma} = 10$ and $y_v(0) = 0.4$ and in column (b) $\tilde{\Gamma} = 20$ and $y_v(0) = 0.4$. Below the solitary wave is an open circle which denotes the position of the vortex.

4.2. The effect of horizontal vortex velocity

We have observed that when the vortex propagates with a velocity which is different from the interfacial waves the interaction between the vortex and the layer is not sustained for long time. In this subsection, we test this idea by considering two very strong vortices, $\tilde{\Gamma} = 10$ and 20 , which are placed in the vorticity layer, $y_v(0) = 0.4$, and propagate downstream three to five times faster than the linear long-wave limit of the linear phase velocity.

In figure 18, the deformation of the interface is shown for $t = 0, 5, 8, 10$. The position of the vortex is indicated by the circle. In column (a), $\tilde{\Gamma} = 20$ and in column (b) $\tilde{\Gamma} = 10$. Despite the large strength of the vortex, the amplitude of the waves does

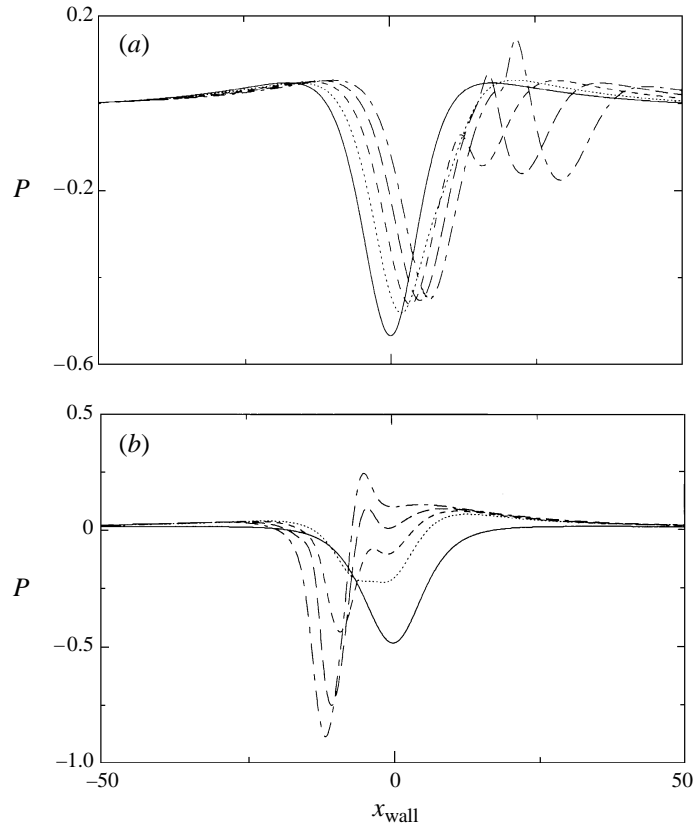


FIGURE 19. The pressure at different streamwise locations, x , along the wall. The solid, dotted, dashed, long-dashed and dot-dashed lines correspond to $t = 0, 5, 10, 15, 20$ respectively and $y_v(0) = 10$. The non-dimensional pressure, $P = p(x) - p(-\infty)$ approaches zero as $|x| \rightarrow \infty$. (a) $\tilde{T} = 40$ and (b) $\tilde{T} = -40$. Note that the interface deformations for the corresponding cases are shown in figures 4 and 10.

not continue to grow with time, and is moderate in size. In both cases, a solitary wave of unchanging form propagates in tandem with the vortex leaving disturbances which entrain thin filaments of irrotational flow deep into the layer far upstream. The increasing distance between the vortex and the upstream disturbances and the unchanging form of the solitary wave suggest a fleeting interaction. Similar results (Atassi *et al.* 1997) were shown to exist when a strong vortex was placed very close to the wall. In this case, the vortex propagated quickly downstream leaving dispersive waves far behind it. Unlike those results, the disturbances here are not small and deep penetration of irrotational flow into the layer is observed far upstream of the vortex.

5. The wall pressure

The wall pressure field can be determined from the velocity field via the momentum equation. The pressure, $p(x)$, takes the form

$$p(x, t) = p(-\infty) - \left[\int_{-\infty}^x \frac{\partial u}{\partial t} dx' + 1/2(u^2 - 1) \right]. \quad (5.1)$$

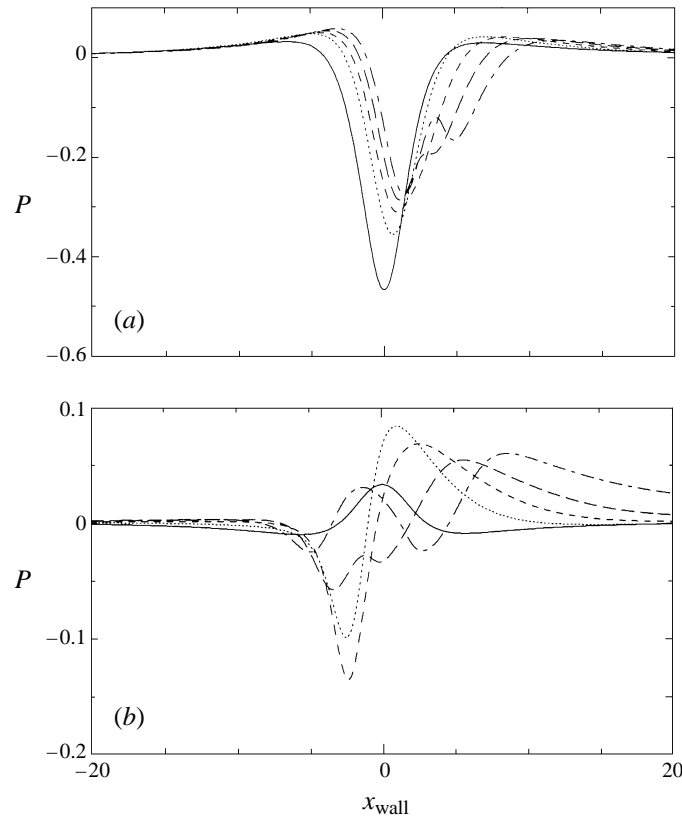


FIGURE 20. As figure 19 but for $y_v(0) = 3$ and (a) $\tilde{\Gamma} = 8$, (b) $\tilde{\Gamma} = -4$. Note that the interface deformation for the corresponding cases is shown in figures 15 and 14.

The wall pressure is computed for four cases for which the interface deformation was computed in the previous section. We examine the effect of a strong vortex–shear layer interaction on the wall pressure. In the first two cases, $\tilde{\Gamma} = \pm 40$ and $y_v(0) = 10$. Recall that when $\tilde{\Gamma} = -40$ a strong interaction was observed which led to the ejection of vorticity into the irrotational flow whereas when $\tilde{\Gamma} = 40$ a weak, waning interaction occurred and wave-like behaviour was observed on the interface. Figure 19 presents the wall pressure at the times $t = 0, 5, 10, 15, 20$. The corresponding plots of the interface deformation are given in figures 4 and 10.

For $\tilde{\Gamma} = -40$, the pressure along the wall starts as a symmetric trough with a peak value of -0.5 directly below the vortex ($x_v = 0$). The pressure decays for large values of $|x|$. As time evolves, the pressure increases near the location of the initial trough to a value of nearly 0.25 and a low-pressure region develops upstream nearly reaching a value of -0.9 . This corresponds to more than a tripling in magnitude of the initial maximum pressure. The x -location of this low-pressure region coincides with the x -location of the region of ejected vorticity shown in figure 10.

When $\tilde{\Gamma} = 40$ an initially symmetric pressure disturbance with a minimum value near -0.6 lies directly below the vortex. Again the pressure decays for large $|x|$. As time evolves the magnitude of the initial pressure trough decreases slightly and a small pressure disturbance develops and propagates downstream of the trough. The

x -location of this pressure disturbance coincides with the solitary wave that moves downstream as seen in figure 4.

In figure 20, the pressure is plotted at the times $t = 0, 5, 10, 15, 20$ for cases where $\tilde{\Gamma} = -4, 8$ and $y_v(0) = 3$. Recall that when $\tilde{\Gamma} = -4$ (figure 14), a strong interaction was observed and a narrow strip of vorticity was ejected into the irrotational flow whereas for $\tilde{\Gamma} = 8$ (figure 16), a large disturbance was formed but the interaction between the vortex and the layer diminished with time. Figure 20(b) ($\tilde{\Gamma} = -4$) shows a small pressure peak lying directly below the vortex. For $0 \leq t \leq 10$ this pressure peak grows for $x > 0$ and propagates downstream. Upstream ($x < 0$) a significant drop in pressure is observed near $x = -4$. By $t = 10$ this new pressure trough reaches an extremum and for larger times decreases while a smaller wave emerges from the main disturbance and propagates downstream. Recalling the corresponding plot of the interface deformation, figure 14, we see that the x -location of the pressure drop coincides with that of the ejecting and overturning vortical disturbance. For $t > 10$ we observe that the mound of vorticity is being strained and becomes thinner in vertical extent and longer in horizontal extent with time. This stretching of the mound-like disturbance into a thin filament of vorticity stretching from $-5 < x < 2$ results in a broadening and a decrease in the magnitude of wall pressure below it. Moreover, the subsequent entrainment of irrotational flow results in a large increase in the pressure below it. The wall pressure at $0 < x < 5$ changes from a single trough to several pressure waves of smaller amplitude. Interestingly, the wall pressure in this case is quite different from that corresponding to $\tilde{\Gamma} = -40$ and $y_v(0) = 10$ (figure 10) where the mound of vorticity is not stretched in the streamwise direction and instead continues to accumulate in a relatively localized region near $x = -15$. In the present case, overturning and entrainment of irrotational flow into the layer dominate the long-time behaviour resulting in an increase in the pressure minimum.

When $\tilde{\Gamma} = 8$, a symmetric pressure trough forms with its maximum amplitude initially lying below the vortex. As time evolves, the magnitude of the pressure minimum decreases and propagates slowly downstream. Another pressure disturbance begins to emerge downstream of the main disturbance and propagates downstream. The increase in pressure appears to be related to the entrainment and penetration of irrotational flow into the layer as observed in figure 16.

5.1. The spectral decomposition of the wall pressure

It is interesting to study how the spectrum is modified by the unsteady interaction. As a result, we compute the spectral decomposition of the wall pressure for the two cases $\tilde{\Gamma} = \pm 40$, $y_v(0) = 10$.

Figure 21 shows the wall pressure spectrum where column (a) corresponds to $\tilde{\Gamma} = -40$ and (b) to $\tilde{\Gamma} = 40$. Recall that the corresponding wall pressure plots are shown in figure 19. When $\tilde{\Gamma} = -40$, the initial spectrum shows a maximum at low wavenumbers and then a rapid decay at higher wavenumbers. As the wall pressure evolves, a cascade to higher wavenumbers is observed and is indicated by the broadening of the spectrum. This is consistent with the wall pressure shown in figure 18 which indicates the steepening and growth of several smaller scale disturbances. When $\tilde{\Gamma} = 40$, figure 19 shows that the wall pressure breaks up into several disturbances over time. The spectrum initially has its maximum at low wavenumbers and rapidly decays at higher wavenumbers. As the vortex-layer interaction evolves with time, several new harmonics in the spectrum are observed. It is suggested that these new harmonics may be associated with the dispersive waves. Furthermore, this suggests

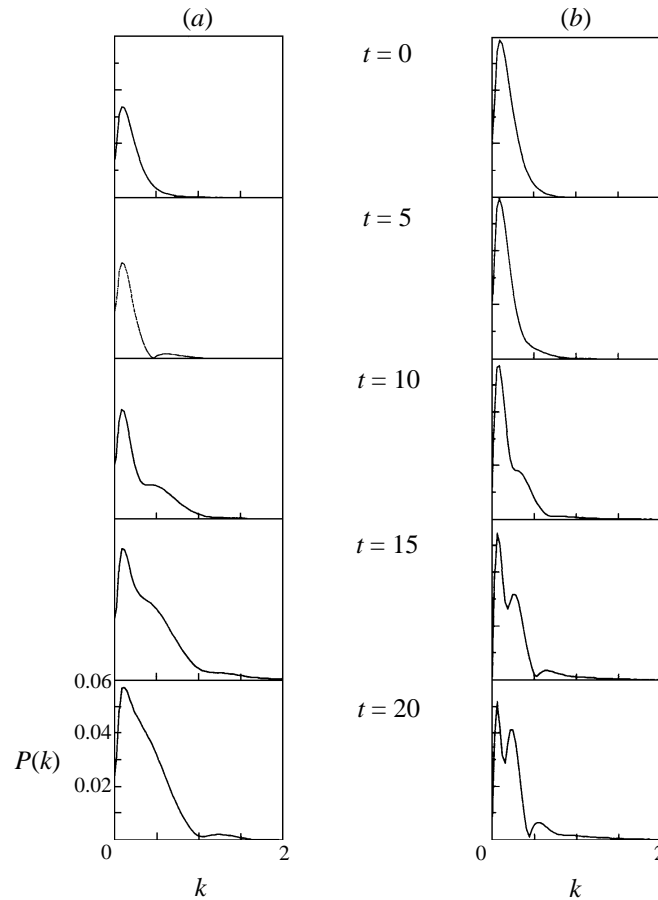


FIGURE 21. The spectral composition of the wall pressure: (a) $\tilde{\Gamma} = -40$ and (b) $\tilde{\Gamma} = 40$. In both cases, $y_v(0) = 10$.

that forcing vortices which interact with wall-bounded vorticity layers may modify the structure of the turbulence.

6. Discussion and conclusions

The unsteady interaction between a point vortex and a wall-bounded layer of vorticity has been studied as a model problem for momentum and energy transfer between rotational and irrotational flows. A variety of behaviour has been observed to exist ranging from dispersive and solitary waves to ejection of vorticity and entrainment of irrotational flow. We have examined several cases where the sign of the vortex circulation was changed for similar magnitudes of the vortex strength. Under conditions where the vortex induces the leading-order velocity field on the interface and the interaction between the vortex and the layer is neglected (the linear and very strong vortex cases: §§ 3.3.1–3.3.3) only the sign of the interface shape changes when the vortex orientation is varied, see equations (3.38) and (3.50). However when the self-interaction of the layer balances with the velocity induced by the vortex, very different solutions may arise depending upon the sign of $\tilde{\Gamma}$. When $\tilde{\Gamma} < 0$, a stationary point along the interface occurs for a smaller value of $|\tilde{\Gamma}|$ than

for $\tilde{\Gamma} > 0$ (3.60). Moreover, in this case, the horizontal vortex velocity is closer to the velocity of the interfacial disturbances. As a result, the unsteady interaction between the vortex and the layer is sustained for longer time. This result is consistent with the small-amplitude results obtained in Atassi *et al.* (1997) where it was found that small-amplitude disturbances resonated with the vortex when the phase velocity of the interfacial waves coincided with the horizontal vortex velocity.

Although the deformation of the interface varies for each case, we classify the phenomena as two types. When the interaction between the vortex and the layer is not strong and/or not sustained, *wave-like* behaviour is observed. Otherwise, when a strong interaction occurs, vorticity is *ejected* away from the wall and the irrotational flow is *entrained* towards the wall. A number of general conclusions regarding the conditions for strong interaction and its dynamical consequences may be drawn from this study. Sustained unsteady interaction is most likely to occur when (i) the vortex propagates with a horizontal velocity close to that of the interfacial waves, and (ii) the sign of the vortex circulation is opposite to the vorticity in the layer.

Condition (i) follows from the property that the velocity induced by regions of vorticity is inversely proportional to the distance separating them. Thus, if the vortex propagates with a horizontal velocity which is different from that of the interfacial disturbances the distance between them will grow with time and the unsteady interaction will diminish with time. Conversely, when the vortex propagates with the interfacial wave velocity a strong interaction occurs.

Condition (ii) was observed numerically and is supported by the analytical long-wave approximation results showing that the initial mechanism for the ejection of vorticity is the presence of a stationary point along the interface. A criterion for the presence of a stationary point is derived and shows that such a point occurs more easily when the vortex rotation is opposite to (180° out of phase) the vorticity of the layer.

The wall pressure was computed and its spectral decomposition analysed to study the dynamical consequences of the ejection of vorticity. An extremum in the wall pressure was observed to form at a location which coincided with that of the growing blob of vorticity.

Other work (Legras & Dritschel 1993; Trieling 1996) has studied the evolution of patches of vorticity in the presence of a straining flow or adverse shear. These studies have indicated that the outer edges of the patch form steepening fronts of vorticity that are eventually stripped away from the patch. They considered patches with both distributed and uniform vorticity distributions. In both cases they found that the important parameter for vortex stripping was the ratio of the strain rate to the maximum vorticity in the layer and they found that the 'stripping of the vortex' occurs at a weaker strain rate when the distribution of vorticity is non-uniform. In this paper, we consider a very different geometry but the results suggest that when a strong interaction between the vortex and the layer occurs a process similar to vortex stripping results in the ejection of vorticity into the irrotational flow. During this process, a region of vorticity is pulled away from the shear layer, becoming narrower as it is ejected into the irrotational flow. The ejection of vorticity was observed to extend up to six times the initial layer thickness. However, beyond these times steep gradients exist which should be smoothed by viscosity and may act to pinch off the thin filament resulting in an island of very concentrated vorticity. This process and these observations add support to the idea that strong unsteady interactions between regions of vorticity lead to the formation of isolated, thin filaments of vorticity which are observed in many two-dimensional flows. The presence of these islands of

concentrated vorticity act to transfer momentum between the outer irrotational flow and the vorticity layer suggesting a mechanism whereby kinetic energy from the mean flow is converted into turbulent fluctuations which cascade to higher wavenumbers. Moreover, in qualitative agreement with turbulent boundary layer observations, strong unsteady interaction is more likely when the rotation of the vortex is counter to the mean vorticity near the wall.

Partial support by NSF grant CTS-9206828 and the Pentair Teaching Fellowship is gratefully acknowledged. Thanks to Professor Richard Lueptow for reading the manuscript and his insightful comments and thanks to Dr. Reuben Trieling for referring me to some experimental work on vortex interactions near coastlines. The author also wishes to thank professors Andrew Bernoff and Seth Lichter for their support.

REFERENCES

- ATASSI, O. V. 1997 The nonlinear interaction between a vortex and a wall-bounded vorticity layer. PhD dissertation, Northwestern University.
- ATASSI, O. V., BERNOFF, A. J. & LICHTER, S. 1997 The interaction of a point vortex with a wall-bounded vortex layer. *J. Fluid Mech.* **143**, 169–195.
- BALAGONDAR, P. M., MASLOWE, S. A. & MELKONIAN, S. 1987 The propagation of finite-amplitude waves in a model boundary layer. *Stud. Appl. Maths* **76**, 169–185.
- BELL, G. I. 1990 Interaction between vortices and waves in a simple model of geophysical flow. *Phys. Fluids* **2**, 575–586.
- BENJAMIN, T. B. 1967 Internal waves of permanent form in fluids of great depth. *J. Fluid Mech.* **29**, 559–592.
- DAVIS, R. E. & ACRIVOS, A. 1967 Solitary internal waves in deep water. *J. Fluid Mech.* **29**, 593–607.
- DOLIGALSKI, T. L. & WALKER, J. D. A. 1984 The boundary layer induced by a convected two-dimensional vortex. *J. Fluid Mech.* **139**, 1–28.
- DRITSCHER, D. G. 1988 Contour surgery: a topological reconnection scheme for extended calculations using contour dynamics. *J. Comput. Phys.* **77**, 240–266.
- FALCO, R. E. 1977 Coherent motions in the outer region of turbulent boundary layers. *Phys. Fluids* **20**, 124–132.
- FALCO, R. E. 1991 A coherent structure model of the turbulent boundary layer and its ability to predict Reynolds number dependence. *Phil. Trans. R. Soc. Lond. A* **336**, 103–129.
- IKEDA, M. & APEL, J. R. 1981 Mesoscale eddies detached from spatially growing meanders in an eastward-flowing oceanic jet using a two-layer quasi-geostrophic model. *J. Phys. Oceanogr.* **11**, 1638–1661.
- JIMENEZ, J. & ORLANDI, P. 1993 The rollup of a vortex layer near a wall. *J. Fluid Mech.* **248**, 297–313.
- KACHANOV, Y. S., RHYZHOV, O. S. & SMITH, F. T. 1993 Formation of solitons in transitional boundary layers: theory and experiment. *J. Fluid Mech.* **251**, 273–297.
- LEGRAS, B. & DRITSCHER, D. 1993 Vortex stripping and the generation of high vorticity gradients in two-dimensional flows. *Appl. Sci. Res.* **51**, 445–455.
- LIU, H. T., SIMPSON, J. J. & SCHEDVIN, J. C. 1988 A preliminary laboratory study of the lateral entrainment of non-local waters by a subsurface mesoscale eddy. *Exps. Fluids* **6**, 217–227.
- MILNE-THOMSON, L. M. 1968 *Theoretical Hydrodynamics*. Macmillan.
- MYOSE, R. Y. & BLACKWELDER, R. F. 1994 On the role of the outer region in the turbulent-boundary-layer bursting process. *J. Fluid Mech.* **259**, 345–373.
- PULLIN, D. I. 1981 The nonlinear behaviour of a constant vorticity layer at a wall. *J. Fluid Mech.* **108**, 401–421.
- PULLIN, D. I., JACOBS, P. A., GRIMSHAW, R. H. J. & SAFFMAN, P. G. 1989 Instability and filamentation of finite-amplitude waves on vortex layers of finite thickness. *J. Fluid Mech.* **209**, 359–384.
- RAYLEIGH, LORD 1887 On the stability or instability of certain fluid motions, II. In *Scientific Papers*, vol. 3, pp. 17–23. Cambridge University Press.

- ROBINSON, S. K. 1991 Coherent motions in the turbulent boundary layer. *Ann. Rev. Fluid Mech.* **23**, 601–639.
- ROSHKO, A. 1976 Structure of turbulent shear flows: a new look. *AIAA J.* **14**, 1349–1357.
- STERN, M. E. & FLIERL, G. R. 1987 On the interaction of a vortex with a shear flow. *J. Geophys. Res.* **92**, 10733–10744.
- STERN, M. E. & PRATT, L. J. 1985 Dynamics of vorticity fronts *J. Fluid Mech.* **161**, 513–532.
- REUBEN, R. R. Two-dimensional vortices in strain and shear flows. PhD dissertation, Eindhoven University of Technology.
- ZABUSKY, N. J., HUGHES, M. H. & ROBERTS, K. V. 1979 Contour dynamics for the euler equations in two dimensions. *J. Comput. Phys.* **30**, 96–106.